Cryo-electron tomography of *C. elegans* mitochondria reveals how the ATP synthase dimer interface shapes crista membranes

Emma Buzzard[1,2], Mathew McLaren[1,2], Piotr Bragoszewski[3], Andrea Brancaccio[4,5], Holly Ford[5], Bertram Daum[1,2], Patricia Kuwabara[5], Ian Collinson[5] & Vicki A.M. Gold[1,2,*].

1 Living Systems Institute, University of Exeter, Exeter, UK.

2 Faculty of Health and Life Sciences, University of Exeter, Exeter, UK.

3 Nencki Institute of Experimental Biology, Polish Academy of Sciences, Warsaw, Poland.

4 Institute of Chemical Sciences and Technologies "Giulio Natta", Department of Chemical Sciences and Materials Technologies, National Research Council (CNR), Milan, Italy.

5 School of Biochemistry, University of Bristol, BS8 1TD, UK.

*corresponding author: Vicki Gold; +44 (0)1392 727454; v.a.m.gold@exeter.ac.uk

Classification: Biological Sciences, Biochemistry

Keywords: Mitochondria, ATP synthase, Cryo-electron tomography, Sub-tomogram averaging, AlphaFold.

Abstract

Mitochondrial ATP synthases form rows of dimers, which induce membrane curvature to give cristae their characteristic lamellar or tubular morphology. The angle formed between the central stalks of ATP synthase dimers varies between species. Using cryo-electron tomography and sub-tomogram averaging, we determined the structure of the ATP synthase dimer from the nematode worm *C. elegans.* We showed that the angle formed by the ATP synthase dimer is different to previously determined structures. The consequences of species-specific differences at the dimer interface were investigated by comparing mitochondrial morphology between *C. elegans* and *S. cerevisiae*. We reveal that a larger ATP synthase dimer angle in *C. elegans* is consequent with more lamellar (flatter) cristae compared to yeast. The underlying cause of this difference was investigated by generating an atomic model of the *C. elegans* ATP synthase dimer by homology modelling and comparing it to an existing *S. cerevisiae* structure. We reveal extensions and rearrangements of *C. elegans* subunits that maintain the dimer interface. We propose that increased dimer angles resulting in flatter cristae could provide an energetic advantage for species that inhabit variable-oxygen environments.

Significance Statement

ATP synthase, the world's smallest rotary motor, generates the energy required for all living processes. The universal formation of ATP synthase dimers in mitochondria induces membrane curvature and cristae formation, generating the famously convoluted inner mitochondrial membrane that maximises ATP production. Intriguingly, the angle between ATP synthase dimers varies between species. Here, we report the discovery of a novel ATP synthase dimer angle in mitochondria from the nematode worm *C. elegans,* identify a relationship between dimer angle and crista membrane morphology, and exploit AlphaFold homology modelling to investigate associated structural changes. In summary, we have taken steps towards understanding the importance of subunit composition at the ATP synthase dimer interface, providing insights into the origins of this evolutionary divergence.

Main Text

Introduction

The F_1F_o ATP synthase is a molecular motor ubiquitous to all living organisms. This machine is required for the essential conversion of an electrochemical gradient into the universal energy currency ATP (1). The ATP synthase is composed of a catalytic F_1 head connected to a membrane-embedded F_o motor by a central stalk; the entire assembly is visualised as a lollipop shape when examined by electron microscopy (2, 3). The central stalk transmits the torque generated by rotation of F_o to the F_1 head, and a peripheral stalk acts as an elastic spring, ensuring malleable coupling between F_1 and F_o (4). Mitochondrial ATP synthases across species share the same complement of core subunits with varying nomenclature (Table S1) (5, 6). Here, we use the *C. elegans* nomenclature, exceptions being use of the *S. cerevisiae* naming system for subunits missing in worms. The F_1 head is comprised of α and β subunits, the central stalk of γ, δ and ε subunits, the peripheral stalk of b d, F_6 and oligomycin sensitivity conferral protein (OSCP) subunits, and the F_o motor contains the c-ring and subunit a.

Mitochondrial ATP synthases are capable of assembling into dimers (7), of which there are 4 types (8): Type I is present in both multicellular (9–11) and unicellular organisms (12) and types II-IV are present in various unicellular organisms (13–18), reviewed in (8). When compared to type II-IV dimers, previously studied type I dimers contain an additional set of subunits at the dimer interface: e, f, g, i/j, k and 8 (8). Based on biochemical and imaging experiments, subunits e and g were shown to be essential for dimer formation (7, 11, 19–21). Dimers of ATP synthase assemble into oligomeric rows (or ribbons) along the curved ridges of crista membranes, observed by cryo-electron tomography (cryoET) (9, 11, 22). This oligomerisation (formation of dimer rows) is mediated by an ancestral motif in subunits e and g (20, 21) with assistance from subunit k (5, 23, 24). Formation of dimer rows is required for crista membrane curvature, and thus maintenance of lamellar or tubular shaped cristae (11, 12). Deformation of cristae into balloon-like structures was observed in *S. cerevisiae* after knockdown of interface subunits e or g (11) and in ageing *P. anserina,* when dimers disassociated into monomers (12). Moreover, molecular simulations indicated

that ATP synthase dimers have an innate propensity to induce membrane curvature (25). This was confirmed experimentally when dimers reconstituted into liposomes spontaneously self-assembled into oligomeric rows to engender this curvature, maintaining identical dimer angles to those observed in whole mitochondria (26).

In situ structures of type I ATP synthase dimers have been determined from native membranes (12, 25–28). Mammals and fungi both display an average angle between the dimer heads of ~86° (27). Interestingly, higher-resolution single particle analysis of the purified bovine ATP synthase dimer reveals that dimer angles likely vary around this average (between 76° and 95°), depending on catalytic state (29). Further atomic-detail structures of purified mitochondrial type I ATP synthase dimers have also been determined from mammals (*Bos taurus* (23) and fungi (*S. cerevisiae* (30) and *Y. lipolytica* (22)). The structure and organisation of ATP synthase dimers have thus been studied across a range of different species, yet our knowledge of invertebrates is lacking. The free living nematode worm *C. elegans* is a well-established model system for the study of invertebrate cell and developmental biology (31), including the role of mitochondria in metabolism, health, disease and aging (32). To complement *in vivo* physiological studies, intact mitochondria can be stably prepared (33, 34) for biochemical and structural analyses (35). Interestingly, studies have shown that nematodes lack the dimer-specific subunits i/j, k (36) and 8 (37) found in mammals and fungi (Table S1). Subunit 8 is encoded by one of two overlapping ATP synthase genes on the mitochondrial genome (38). Proteins encoded on the mitochondrial genome are translated from essential genes (39, 40); thus it follows that subunit 8 is likely to be essential for respiration in mammals and fungi. The lack of dimer-specific subunits in *C. elegans* provides a unique opportunity to investigate how certain subunits influence ATP synthase dimer angles and mitochondrial morphology.

In this study, we employed cryoET and sub-tomogram averaging to reveal the structure and organisation of the *C. elegans* ATP synthase, revealing a novel average dimer angle of 105°. We compared mitochondria from both *C. elegans* and *S. cerevisiae* to investigate the relationship between ATP synthase dimer angle and crista morphology. Finally, we used AlphaFold (41) to predict how protein chains in the *C. elegans* ATP

synthase dimer are arranged. This allowed us to analyse changes at the dimer interface and postulate the cause of differences in angle. We speculate that an evolutionary divergence at the dimer interface and corresponding widening of the dimer angle may be an adaptation to more variable oxygen environments.

Results

The architecture of the *C. elegans* ATP synthase dimer

To determine the arrangement and architecture of ATP synthase dimers in *C. elegans*, tomograms of whole mitochondria (Fig. 1A) and of isolated crista membranes (Fig. 1B) were analysed. ATP synthases were unambiguously identified by the characteristic lollipop shape of the 10 nm diameter F_1 heads positioned ~10 nm away from the membrane. We confirmed the presence of oligomeric ATP synthase dimer ribbons, localised at the sharp curved ridges of crista membranes, in both samples (Fig. 1A, B). Due to the obscuring presence of a dense matrix in whole mitochondria, many more dimers could be visualised in crista membrane samples. Therefore, 3,234 dimer pairs were extracted from the crista membrane data for sub-tomogram averaging. After classification, a map of the *C. elegans* ATP synthase dimer was determined from 1,755 dimer pairs (Fig. 1C, Fig. S1, S2). Both the central and peripheral stalks were resolved clearly.

Previous studies have revealed a type I dimer angle of ~86° across a range of mammalian and fungal species (12, 25–28) . The architecture of the *C. elegans* ATP synthase dimer is unlike any other species studied so far, with an average angle of 105° between the dimer heads (Fig. 2A). A comparison to a sub-tomogram average of the *S. cerevisiae* dimer (42), revealed that the wider dimer angle in *C. elegans* corresponds with a sharper angle of membrane curvature (50° compared to 74°) (Fig. 2B). Accordingly, opposing sides of the *C. elegans* crista membranes are in closer proximity than in *S. cerevisiae* (16.5 nm compared to 20 nm). Intriguingly, the dimer interface in the *C. elegans* map was visually remarkably different to its *S. cerevisiae* counterpart (Fig. 2B), and indeed all other type I dimers studied to date (12, 25–28). This could be due to the different complement of dimer interface subunits present in *C. elegans* compared to *S. cerevisiae* (Table S1, Fig. 2C). We also analysed the inter-dimer distance and angle

between dimer heads in consecutive dimers in the oligomeric rows. This revealed an inter-dimer distance of 12.5 nm and angle between dimer heads of 20°. Despite differences in dimer angle, these values are similar to those reported previously for the type II dimer from green algae (*Polytomella* sp.) (26) (Fig. S3), suggesting that dimer angle does not influence oligomerisation of ATP synthases into rows.

A wider dimer angle in *C. elegans* corresponds to flatter cristae

We hypothesised that the wider dimer angle associated with sharper membrane curvature in the *C. elegans* ATP synthase dimer (Fig. 2B) would produce flatter cristae with a larger surface area to volume ratio. To test this, tomographic data of whole mitochondria from *C. elegans* and *S. cerevisiae* were collected and quantified. Qualitatively, *C. elegans* mitochondria have more lamellar shaped (or flatter) cristae, with sharp curved ridges, compared to mitochondria from *S. cerevisiae* (Fig. 3A, 3B, Movie S1 & S2). The surface area and volume of the crista membranes were quantified, to reveal that the surface area to volume ratio of the average crista membrane was significantly higher (~1.5 fold, **** $p \leq 0.0001$) in *C. elegans* than in *S. cerevisiae* (Fig. 3C). In accordance with this, the average crista width in *C. elegans* (~10 nm) was half the width of cristae in *S. cerevisiae* (~20 nm) (Fig. 3D, E and F). We speculated that narrower cristae in *C. elegans* may allow more efficient membrane packing into the mitochondrial volume. However, no significant difference was found between the total crista volume relative to mitochondrial volume between the two organisms (Fig. 3G). In summary, this suggests that dimer angle exerts influence on mitochondrial morphology at the level of membrane curvature, but this does not alter membrane packing.

Mitochondria are dynamic organelles, and crista morphology can be influenced by a wide range of factors such as metabolic state (43–45). However, the average ATP synthase dimer angle remains consistent when imaged in membranes or on purification in detergent (27, 29). To ensure that morphological differences observed here in whole mitochondria were not a result of different preparation conditions, we also measured the degree of membrane curvature in isolated cristae containing *C. elegans* and *S. cerevisiae* ATP synthase dimers. Our results were consistent with the results obtained *in situ*, with a shorter

crista width observed for the *C. elegans* dimer average (Fig. 2B). This indicates that the dimer angle remains consistent, regardless of how the sample was prepared or analysed.

A unique arrangement of subunits at the *C. elegans* dimer interface

We observed additional density at the *C. elegans* dimer interface (Fig. 2B), which has not been observed in other type I structures determined to date (27). Nematodes are missing subunit 8 (37) (Table S1, Fig. 2C), which plays an key structural role in other species (22, 23, 30, 46) and is considered essential for respiration (39, 40). Therefore, it is likely that considerable rearrangements at the dimer interface would need to occur to account for the lack of subunit 8; this could contribute to the observed change of dimer angle. To explore this possibility, we performed multisequence alignments with *C. elegans, S. cerevisiae* and *B. taurus* (47–49). This revealed extensions in the 3 *C. elegans* subunits located at the dimer interface (e, f and g), and in 3 of the 4 subunits in the peripheral stalk (b, d and F_6) (Fig. S4). Mass spectrometry was used to confirm that the extensions identified by sequence in the dimer interface subunits are present in the mature proteins (Fig. S5).

To position the dimer interface subunits in the *C. elegans* ATP synthase, we used AlphaFold (41) to predict the structures of individual subunits and build a homology model. The mean pLDDT score (a per-residue measure of local confidence on a scale from 0 – 100) of each AlphaFold prediction was > 70 (Table S2, Fig. S6), and therefore defined as a “confident” prediction by the software. Structures of peripheral stalk subunits b, d and F_6 were predicted together as a multimer (50), since individual predictions were not reliable. The predicted structures were then fitted sequentially into a scaffold provided by the *S. cerevisiae* ATP synthase dimer [PDB 6B8H] (Fig. S7, Fig. 4A). Extensions in key *C. elegans* dimer interface subunits relative to their yeast homologues are clearly visible (Fig. S8). The *C. elegans* ATP synthase dimer was then split into monomers and each was fitted sequentially into our sub-tomogram average dimer map (Fig. S7, Fig. 4B), improving the fit considerably (Fig. S9). Our homology model correlated well to the sub-

tomogram averaging map (Fig. S10 and Table S3), allowing a comparison of *S. cerevisiae* and *C. elegans* ATP synthase dimers (Fig. 4C).

Interestingly, the additional density identified in our sub-tomogram averaging map at the dimer interface (Fig. 2B) appears to now be filled by a rearrangement of the extended subunits f and g (Fig. 4C, D & E). In addition, extensions at the base of the peripheral stalk (subunits b, d and F_6) also appear to contribute to the greater mass at the *C. elegans* dimer interface compared to *S. cerevisiae* (Fig. S11). Despite this, there are unfilled gaps at the dimer interface. It is plausible that specific lipids could also contribute to the mass observed, which is in line with their identification and role in stabilisation of the dimer interface (23, 51). We also cannot exclude the possibility that there are additional subunits as yet unidentified in *C. elegans*.

Finally, we fitted the *C. elegans* ATP synthase dimer model into a row of oligomeric dimer pairs along the curved edge of a crista (Fig. 4F, H). This reveals extensive inter-dimer interactions mediated by subunits e and g (Fig, 4G, I and Fig. S12), in agreement with recent work demonstrating the key role that these subunits play a role in oligomerisation / row formation (21).

Discussion

Owing to the essential and universal role of the ATP synthase across eukaryotic species, it is remarkable that the dimeric arrangement can be so variable (10). Until now, the arrangement of ATP synthases in invertebrates was unknown, as was the correlation between dimer angle and whole mitochondrial morphology. In this work, a novel dimer angle for the ATP synthase from the nematode worm *C. elegans* was discovered. By comparing worm and yeast mitochondria, we discovered that a wider ATP synthase dimer angle was associated with a flatter crista membrane morphology. Since dimer row formation is known to be instrumental in formation of curved ridges in crista membranes (11, 12, 26), it is consequent that dimer angle influences the extent of membrane curvature.

AlphaFold is able to predict protein structures with high precision (41). Our homology model of the *C. elegans* ATP synthase dimer thus allowed us to postulate how alterations in the organisation of subunits could influence dimer architecture. The ATP synthase structure is relatively well conserved across species (52), but more weakly at the dimer interface and peripheral stalk (53). In accordance with this, extensions in 3 *C. elegans* subunits (e, f and g) result in the rearrangement of subunits at the dimer interface relative to *S. cerevisiae*. In addition, changes are detected in peripheral stalk components, with a significant N-terminal extension in subunit b, and a range of more subtle gaps and insertions in subunits d and F_6, which bulk out the width of the dimer interface. Some dimer interface subunits present in *S. cerevisiae* (j, k and 8) are absent in *C. elegans.* Whilst it cannot be completely excluded that an as yet unidentified subunit may substitute for 8, we speculate that the absence of 8 in worms (37) highlights an interesting evolutionary divergence. Subunit 8 is usually encoded on the mitochondrial genome, indicating that it is essential (39, 40). Additionally, 8 appears to have a key structural role in joining the dimer interface to the peripheral stalk (22, 23, 30, 46). It is therefore likely that the space vacated by the missing subunit 8 is either resolved by the re-arrangement of neighbouring subunits, or substituted by one of the extensions of the F_O subunits close by (b, d, e, f or g).

Mitochondria have evolved their highly convoluted crista membranes to increase their surface area (54), hence accommodating the maximum amount of respiratory chain complexes. This has made it possible for eukaryotic organisms to deal with higher energy demands than prokaryotes (54). However, we found that the flatter cristae in *C. elegans* relative to *S. cerevisiae* is not associated with more efficient cristae membrane packing into the mitochondrial volume. ATP synthesis is driven by the proton-motive force (PMF) and the efficiency of ATP production is directly proportional to the local proton concentration. It has been suggested that cristae serve as proton concentrators that facilitate a directed flow from the source (respiratory chain) to sink (ATP synthase) (9, 27). On this premise, the concentration effect exerted by the cristae would be directly proportional to the number of protons pumped in a given time and the volume of the crista lumen. It follows that in a flatter crista of equivalent volume to a wider one (e.g. *C. elegans* compared to *S. cerevisiae*), fewer protons would need to be pumped to reach a given concentration, and

hence to reach the PMF required to drive the ATP synthase. In addition, protons have been proposed to preferably migrate from source to sink along membrane surfaces. If this is the case, then reducing the width of the crista space will reduce the solvent volume that the protons can dissipate into, facilitating the efficiency of ATP synthesis. Both of these factors could allow *C. elegans* to maximise energy production in its soil-based habitat (55), where conditions range from near hypoxia to atmospheric (56, 57). Thus, we propose that a wider ATP synthase dimer angle associated with flatter cristae may be paramount for capitalising on ATP production when a higher level of oxygen becomes available, and that a range of angles have evolved to meet the energetic needs of different organisms. Future studies geared towards investigating dimer subunit composition, angle and corresponding crista morphology in a range of species inhabiting different environments will be key. The divergence in ATP synthase dimer architecture relative to yeast and mammalian systems makes *C. elegans* an ideal model system for further investigation of the role of dimer angle in mitochondrial physiology, health and disease.

Conclusions

In this work, we discovered that the *C. elegans* mitochondrial ATP synthase forms a novel dimer interface with an angle between subunits of 105°. We have shown that this unusually wide angle is associated with flatter cristae compared with the yeast *S. cerevisiae.* We conclude that rearrangement of subunits at the dimer interface controls dimer angle and accordingly the extent of membrane curvature. Since an energetic advantage is likely to be proffered by an increased local proton concentration, we speculate that a range of dimer angles may have evolved to alter crista diameter and thus suit bespoke energetic needs.

Materials and Methods

All standard reagents were purchased from Sigma-Aldrich (Burlington, USA).

C. elegans and *S. cerevisiae* culture

The *C. elegans* N2 Bristol strain was maintained at 20°C on 60 mm Nematode Growth Medium (NGM) plates seeded with *E. coli* OP50. For large scale preparations, a semi-synchronised population of *C. elegans* (achieved by starving so that they entered the dauer stage) (58, 59) were grown in a liquid suspension of *E. coli* NA22 in S-basal complete medium (60) at 20°C, shaking at 200 rpm for 3 days to achieve adults. For further details see (34). *S. cerevisiae* 'Bakers's yeast' S288C derivative strains YPH499 were cultured at 19 - 24°C in YPGal or YPG medium (1% w/v yeast extract, 2% w/v bactopeptone, 2% w/v galactose or 3% w/v glycerol) until OD 2-2.5 was reached. For further details see (61).

Mitochondrial isolation

C. elegans and *S. cerevisiae* were both harvested from liquid cultures by low speed centrifugation. *C. elegans* preparation required an additional sucrose flotation step to remove debris. To soften the *C. elegans* cuticle, the pellets underwent collagenase treatment (1 U/ml collagenase, 100 mM Tris-HCl pH 7.4 and 1 mM $CaCl_2$), whilst *S. cerevisiae* pellets underwent dithiothreitol (10 mM DTT, 100 mM Tris-SO4 pH 9.4) and zymolyase treatment (4.5mg/g zymolyase, 1.2 M sorbitol, 20 mM potassium phosphate, pH 7.4) to disrupt the cell wall. Pellets from both species were re-suspended in homogenisation buffers. For *C. elegans*, this was STEG/M (220 mM mannitol, 70 mM sucrose, 5 mM Tris-HCl pH 7.4 and 1 mM EGTA supplemented with 1 mM PMSF in methanol and 1% (w/v) fatty acid-free BSA). For *S. cerevisiae* the homogenization buffer contained 0.6 M sorbitol, 10 mM Tris–HCl pH 7.4, 1 mM PMSF, 0.2% (w/v) BSA, 2 mM magnesium acetate. The re-suspended *C. elegans* or *S. cerevisiae* samples were homogenised in a glass-Teflon Potter homogenisor to break open cells. Both samples were subsequently spun at low speed (750 – 3000 x g for 5-15 minutes) to remove cell debris and nuclei, and then at higher speed (12,000 x g for 15 minutes) to pellet mitochondria. Purified mitochondria were re-suspended in buffers that were

optimised to maintain intact mitochondria: 220 mM mannitol, 70 mM sucrose, 5 mM Tris-HCl pH 7.4 and 1 mM EGTA for *C. elegans* or 250 mM sucrose, 2 mM magnesium acetate, 10 mM Mops, pH 7.2 for *S. cerevisiae*.

Mitochondrial crista membrane isolation

Crista membranes used for the sub-tomogram averaging experiments were generated by successive freeze-thaw cycles of mitochondria at -80°C. To purify mitochondrial membranes from other cellular material, membrane extracts were incubated for 1h at 4°C with an anti-NDUFS3 primary antibody (ab14711; abcam) against the matrix arm of complex I from *C. elegans*, followed by a 3h incubation with an anti-mouse secondary conjugated to a quantum dot emitting at 625 nm (Q22085; Invitrogen). Crista membranes were separated from unbound antibodies and other cellular material on an Optiprep gradient with 10 layers (200 µl volume each) ranging from 0 to 27% v/v of iodixanol in STEG/M buffer, by centrifugation at 80,000 × *g* for 30 min at 4°C using a TLS-55 rotor (Beckman Coulter Inc., Miami, FL, USA). Crista membranes were identified and removed based on fluorescence under a UV lamp. Samples were then diluted in STEG/M buffer to wash out the iodixanol, and spun at 20,000 *x g* for 15 min at 4 °C to pellet the membranes. The enriched cristae were again re-suspended in STEG/M buffer.

Electron cryo-tomography

Whole mitochondria or crista membranes were mixed 1:1 with 10 nm gold fiducials (Aurion, Wageningen, The Netherlands), applied to glow-discharged holey carbon EM grids (Quantifoil, Jena, Germany), and blotted for 5-6 seconds, followed by plunge-freezing in liquid ethane using a Vitrobot Mark IV (ThermoFisher, Massachusetts, USA) for *C. elegans*, or a home-made device for whole *S. cerevisiae* mitochondria. Pre-screening of *C. elegans* grids was carried out using an FEI Tecnai Spirit 120kV microscope (ThermoFisher), with a Oneview CCD Camera (Gatan, Pleasanton, USA). CryoET was performed using the same microscope for whole mitochondria, or using a 200 kV Talos Arctica (ThermoFisher) for crista membranes, equipped with a K2 direct electron detector camera and a GIF

Quantum LS energy filter (Gatan). CryoET of whole *S. cerevisiae* mitochondria was performed using a 300 kV Titan Krios (ThermoFisher), K2 direct electron detector camera and a GIF Quantum LS energy filter (Gatan). Single tilt image series' (±60, step size 1.5° - 2°) were collected at -5 to -8 µm underfocus at nominal magnification of 21,000 x for whole mitochondria and 39,000 x for crista membranes, corresponding to 5.4 and 3.58 Å pixel sizes respectively for *C. elegans*, or 26,000 x for whole mitochondria from *S. cerevisiae*, corresponding to a 4.51 Å pixel size. The total dose per tomogram was ~120 $e^-/Å^2$ for whole mitochondria, and ~80 $e^-/Å^2$ for isolated cristae. Tomograms were aligned using the gold fiducials in IMOD (University of Colorado, United States) (62) and volumes reconstructed via weighted back-projection. Contrast was enhanced by nonlinear anisotropic diffusion (NAD) filtering (63), followed by manual segmentation, also in IMOD. ImageJ (64) was used to generate movies of segmentations generated in IMOD.

Subtomogram averaging

3,234 *C. elegans* ATP synthase dimers were picked manually in IMOD, using NAD-filtered tomograms. Subvolumes containing the ATP synthase dimer were then extracted from tomograms that had not been NAD filtered. These sub-volumes were CTF corrected and imported into Relion 3.1 (65) using the approach and script described in (66). A reference-free initial model was generated using 3 x binned subvolumes and 2,481 dimers were selected by 2D classification for an unbinned refinement. Finally, 1,755 dimers were selected from a 3D classification of this refined model to enter a final round of refinement and post-processing, resulting in a 38.6 Å resolution map. Fig. S1 details the full workflow.

Homology model generation

AlphaFold was used to predict five structural models of each ATP synthase subunit in *C. elegans* based on their mature protein sequence (41). Mature sequences were determined using MitoFates (67) or TargetP-2.0 (68) to predict mitochondrial targeting sequences. All ATP synthase subunits known to be present in *C. elegans* were included, excepting a putative homologue of subunit j, on account of its poor alignment with

other homologues, and absence of any corresponding peptides in mass spectrometry analysis of the *C. elegans* dimer. The structures of peripheral stalk subunits b, d and F_6 were predicted using AlphaFold multimer (50), as the individual predictions were unreliable. The models for each subunit with the highest average pLDDT score were fitted sequentially to a scaffold provided by the atomic model of the *S. cerevisiae* ATP synthase dimer [PDB 6BH8] in ChimeraX (69) using the Matchmaker tool. Where a subunit had more than one isoform, the version with the highest pLDDT score was used. In the case of subunit b, the isoform with the highest pLDDT score is also the only isoform expressed in somatic tissues (70). The resulting structure was divided into monomers, and fitted sequentially into the sub-tomogram average of the *C. elegans* ATP synthase dimer using the “fit in volume” tool in ChimeraX. The workflow is shown in Fig. S7. The resulting homology model was converted into an MRC map using the pdb2mrc command in EMAN2 (71). This map could then be fitted to the sub-tomogram average map of the *C. elegans* dimer for comparison (Fig. S10). The yeast monomeric atomic model [PDB 6CP6] (72) was used for additional analysis in Fig. S8.

Mass spectrometry

The ATP synthase was purified from *C. elegans* mitochondria using a method described previously (73, 74), and analysed by Nano-LC mass spectrometry. Briefly, isolated mitochondria were solubilised and mixed with a His-tagged inhibitor protein IF_1. This suspension was applied to a Nickel column to capture inhibited ATP synthase. The fraction most enriched in ATP synthase subunits was taken for mass spectrometry analysis. Further details are given in Supporting Information.

References

1. P. Mitchell, Chemiosmotic coupling in oxidative and photosynthetic phosphorylation. *Biol. Rev.* **41**, 445–502 (1966).

2. J. L. Rubinstein, Structure of the mitochondrial ATP synthase by electron cryomicroscopy. *EMBO J.* **22**, 6182–6192 (2003).

3. W. C. Y. Lau, L. A. Baker, J. L. Rubinstein, Cryo-EM structure of the yeast ATP synthase. *J. Mol. Biol.* **382**, 1256–1264 (2008).

4. M. Sobti, *et al.*, Cryo-EM structures of the autoinhibited *E. coli* ATP synthase in three rotational states. *Elife* **5**, e21598 (2016).

5. J. He, *et al.*, Assembly of the membrane domain of ATP synthase in human mitochondria. *Proc. Natl. Acad. Sci. USA.* **115**, 2988–2993 (2018).

6. J. Song, N. Pfanner, T. Becker, Assembling the mitochondrial ATP synthase. *Proc. Natl. Acad. Sci. USA.* **115**, 2850–2852 (2018).

7. I. Arnold, Yeast mitochondrial F_1F_o-ATP synthase exists as a dimer: identification of three dimer-specific subunits. *EMBO J.* **17**, 7170–7178 (1998).

8. W. Kühlbrandt, Structure and mechanisms of F-Type ATP synthases. *Annu. Rev. Biochem.* **88**, 515–549 (2019).

9. M. Strauss, G. Hofhaus, R. R. Schröder, W. Kühlbrandt, Dimer ribbons of ATP synthase shape the inner mitochondrial membrane. *EMBO J.* **27**, 1154–1160 (2008).

10. K. M. Davies, *et al.*, Macromolecular organization of ATP synthase and complex I in whole mitochondria. *Proc. Natl. Acad. Sci. USA.* **108**, 14121–14126 (2011).

11. K. M. Davies, C. Anselmi, I. Wittig, J. D. Faraldo-Gómez, W. Kühlbrandt, Structure of the yeast F_1 F_o-ATP synthase dimer and its role in shaping the mitochondrial cristae. *Proc. Natl. Acad. Sci. USA.* **109**, 13602–13607 (2012).

12. B. Daum, A. Walter, A. Horst, H. D. Osiewacz, W. Kühlbrandt, Age-dependent dissociation of ATP

synthase dimers and loss of inner-membrane cristae in mitochondria. *Proc. Natl. Acad. Sci. USA.* **110**, 15301–15306 (2013).

13. M. Vázquez-Acevedo, *et al.*, Dissecting the peripheral stalk of the mitochondrial ATP synthase of chlorophycean algae. *Biochim. Biophys. Acta - Bioenerg.* **1857**, 1183–1190 (2016).

14. A. W. Mühleip, *et al.*, Helical arrays of U-shaped ATP synthase dimers form tubular cristae in ciliate mitochondria. *Proc. Natl. Acad. Sci. USA.* **113**, 8442–8447 (2016).

15. A. W. Mühleip, C. E. Dewar, A. Schnaufer, W. Kühlbrandt, K. M. Davies, *In situ* structure of trypanosomal ATP synthase dimer reveals a unique arrangement of catalytic subunits. *Proc. Natl. Acad. Sci. USA.* **114**, 992–997 (2017).

16. M. G. Montgomery, O. Gahura, A. G. W. Leslie, A. Zíková, J. E. Walker, ATP synthase from *Trypanosoma brucei* has an elaborated canonical F_1 -domain and conventional catalytic sites. *Proc. Natl. Acad. Sci. USA.* **115**, 2102–2107 (2018).

17. K. M. Davies, W. Kühlbrandt, Structure of the catalytic F_1 head of the F_1-F_o ATP synthase from *Trypanosoma brucei. Proc. Natl. Acad. Sci. USA.* **115**, E2906–E2907 (2018).

18. B. J. Murphy, *et al.*, Rotary substates of mitochondrial ATP synthase reveal the basis of flexible F_1-F_o coupling. *Science.* **364**, 6446(2019).

19. I. Arnold, K. Pfeiffer, W. Neupert, R. A. Stuart, H. Schägger, ATP Synthase of yeast mitochondria. *J. Biol. Chem.* **274**, 36–40 (1999).

20. P. Paumard, *et al.*, The ATP synthase is involved in generating mitochondrial cristae morphology. *EMBO J.* **21**, 221–230 (2002).

21. O. Gahura, *et al.*, An ancestral interaction module promotes oligomerization in divergent mitochondrial ATP synthases. *Nat. Commun.* **13**, 5989 (2022).

22. A. Hahn, *et al.*, Structure of a complete ATP synthase dimer reveals the molecular basis of inner mitochondrial membrane morphology. *Mol. Cell* **63**, 445–456 (2016).

23. T. E. Spikes, M. G. Montgomery, J. E. Walker, Structure of the dimeric ATP synthase from bovine

mitochondria. *Proc. Natl. Acad. Sci. USA.* **117**, 23519–23526 (2020).

24. J. He, *et al.*, Assembly of the peripheral stalk of ATP synthase in human mitochondria. *Proc. Natl. Acad. Sci. USA.* **117**, 29602–29608 (2020).

25. C. Anselmi, K. M. Davies, J. D. Faraldo-Gómez, Mitochondrial ATP synthase dimers spontaneously associate due to a long-range membrane-induced force. *J. Gen. Physiol.* **150**, 763–770 (2018).

26. T. B. Blum, A. Hahn, T. Meier, K. M. Davies, W. Kühlbrandt, Dimers of mitochondrial ATP synthase induce membrane curvature and self-assemble into rows. *Proc. Natl. Acad. Sci. USA.* **116**, 4250–4255 (2019).

27. K. M. Davies, *et al.*, Macromolecular organization of ATP synthase and complex I in whole mitochondria. *Proc. Natl. Acad. Sci. USA.* **108**, 14121–14126 (2011).

28. W. Kühlbrandt, Structure and function of mitochondrial membrane protein complexes. *BMC Biol.* **13**, 89 (2015).

29. T. E. Spikes, M. G. Montgomery, J. E. Walker, Interface mobility between monomers in dimeric bovine ATP synthase participates in the ultrastructure of inner mitochondrial membranes. *Proc. Natl. Acad. Sci. USA.* **118**, 8 (2021).

30. H. Guo, S. A. Bueler, J. L. Rubinstein, Atomic model for the dimeric F_o region of mitochondrial ATP synthase. *Science.* **358**, 936–940 (2017).

31. M. Markaki, N. Tavernarakis, Modeling human diseases in *Caenorhabditis elegans*. *Biotechnol. J.* **5**, 1261–1276 (2010).

32. K. Yasuda, *et al.*, Age-related changes of mitochondrial structure and function in *Caenorhabditis elegans*. *Mech. Ageing Dev.* **127**, 763–770 (2006).

33. L. I. Grad, L. C. Sayles, B. D. Lemire, Isolation and functional analysis of mitochondria from the nematode *Caenorhabditis elegans*. *Methods Mol. Biol.* **272**, 51-66 (2007).

34. A. Knapp-Wilson, *et al.*, Maintenance of complex I and its supercomplexes by NDUF-11 is

essential for mitochondrial structure, function and health. *J. Cell Sci.* **134**, jcs258399 (2021).

35. R. R. Murfitt, K. Vogel, D. R. Sanadi, Characterization of the mitochondria of the free-living nematode, *Caenorhabditis elegans. Comp. Biochem. Physiol. Part B Comp. Biochem.* **53B**, 423–430 (1976).

36. W. Y. Tsang, B. D. Lemire, The role of mitochondria in the life of the nematode, *Caenorhabditis elegans. Biochim. Biophys. Acta - Mol. Basis Dis.* **1638**, 91–105 (2003).

37. R. Okimoto, J. L. Macfarlane, D. O. Clary, D. R. Wolstenholme, The mitochondrial genomes of two nematodes, *Caenorhabditis elegans* and *Ascaris suum*. *Genetics* **130**, 471–498 (1992).

38. I. M. Fearnley, J. E. Walker, Two overlapping genes in bovine mitochondrial DNA encode membrane components of ATP synthase. *EMBO J.* **5**, 2003–2008 (1986).

39. J. Shen, *et al.*, Oxygen consumption rates and oxygen concentration in Molt-4 cells and their mtDNA Depleted (ρ0) Mutants. *Biophys. J.* **84**, 1291–1298 (2003).

40. J. A. Stuart, M. F. Brown, Mitochondrial DNA maintenance and bioenergetics. *Biochim. Biophys. Acta - Bioenerg.* **1757**, 79–89 (2006).

41. J. Jumper, *et al.*, Highly accurate protein structure prediction with AlphaFold. *Nature* **596**, 583–589 (2021).

42. K. M. Davies, *et al.*, Visualization of ATP synthase dimers in mitochondria by electron cryo-tomography. *J. Vis. Exp.*, e51228 (2014).

43. C. A. Mannella, Structure and dynamics of the mitochondrial inner membrane cristae. *Biochim. Biophys. Acta - Mol. Cell Res.* **1763**, 542–548 (2006).

44. G. C. Pereira, *et al.*, Hexokinase II dissociation alone cannot account for changes in heart mitochondrial function, morphology and sensitivity to permeability transition pore opening following ischemia. *PLoS One* **15**, e0234653 (2020).

45. C. R. Hackenbrock, Ultrastructural bases for metabolically linked mechanical activity in mitochondria I. Reversible ultrastructural changes with change in metabolic steady state in

isolated liver mitochondria. *J. Cell Biol.* **30**, 269–297 (1966).

46. J. Gu, *et al.*, Cryo-EM structure of the mammalian ATP synthase tetramer bound with inhibitory protein IF1. *Science.* **364**, 1068–1075 (2019).

47. F. Sievers, *et al.*, Fast, scalable generation of high-quality protein multiple sequence alignments using Clustal Omega. *Mol. Syst. Biol.* **7**, 539 (2011).

48. M. Goujon, *et al.*, A new bioinformatics analysis tools framework at EMBL-EBI. *Nucleic Acids Res.* **38**, W695–W699 (2010).

49. H. McWilliam, *et al.*, Analysis Tool Web Services from the EMBL-EBI. *Nucleic Acids Res.* **41**, W597–W600 (2013).

50. R. Evans, *et al.*, Protein complex prediction with AlphaFold-Multimer. *bioRxiv* (2021) https:/doi.org/10.1101/2021.10.04.463034 (November 30, 2021).

51. A. Mühleip, S. E. McComas, A. Amunts, Structure of a mitochondrial ATP synthase with bound native cardiolipin. *Elife* **8**, e51179 (2019).

52. M. Yoshida, E. Muneyuki, T. Hisabori, ATP synthase - a marvellous rotary engine of the cell. *Nat. Rev. Mol. Cell Biol.* **2**, 669–677 (2001).

53. G. M. Courbon, J. L. Rubinstein, CryoEM Reveals the complexity and diversity of ATP synthases. *Front. Microbiol.* **13**, 864006 (2022).

54. N. Lane, W. Martin, The energetics of genome complexity. *Nature* **467**, 929–934 (2010).

55. E. Moreno, A. McGaughran, C. Rödelsperger, M. Zimmer, R. J. Sommer, Oxygen-induced social behaviours in *Pristionchus pacificus* have a distinct evolutionary history and genetic regulation from *Caenorhabditis elegans*. *Proc. R. Soc. B Biol. Sci.* **283**, 20152263 (2016).

56. K. H. Tan, *Principles of soil chemistry*, 4th Ed. (2011)

57. W. Wang, *et al.*, Effect of oxygen concentration on the composting process and M maturity. *Compost Sci. Util.* **15**, 184–190 (2007).

58. N. Fielenbach, A. Antebi, *C. elegans* dauer formation and the molecular basis of plasticity. *Genes Dev.* **22**, 2149–2165 (2008).

59. Karp X. Working with dauer larvae. (August 9, 2018), *WormBook,* ed. The *C. elegans* Research Community, WormBook, doi/10.1895/wormbook.1.180.1, http://www.wormbook.org

60. Stiernagle, T. Maintenance of *C. elegans* (February 11, 2006), *WormBook*, ed. The *C. elegans* Research Community, WormBook, doi/10.1895/wormbook.1.101.1, http://www.wormbook.org

61. V. A. Gold, P. Chroscicki, P. Bragoszewski, A. Chacinska, Visualization of cytosolic ribosomes on the surface of mitochondria by electron cryo-tomography. *EMBO Rep.* **18**, 1786–1800 (2017).

62. J. R. Kremer, D. N. Mastronarde, J. R. McIntosh, Computer visualization of three-dimensional image data using IMOD. *J. Struct. Biol.* **116**, 71–76 (1996).

63. A. S. Frangakis, R. Hegerl, Noise reduction in electron tomographic reconstructions using nonlinear anisotropic diffusion. *J. Struct. Biol.* **135**, 239–250 (2001).

64. C. A. Schneider, W. S. Rasband, K. W. Eliceiri, NIH Image to ImageJ: 25 years of image analysis. *Nat. Methods* **9**, 671–675 (2012).

65. S. H. W. Scheres, Amyloid structure determination in RELION -3.1. *Acta Crystallogr. Sect. D Struct. Biol.* **76**, 94–101 (2020).

66. T. A. M. Bharat, S. H. W. Scheres, Resolving macromolecular structures from electron cryo-tomography data using subtomogram averaging in RELION. *Nat. Protoc.* **11**, 2054–2065 (2016).

67. Y. Fukasawa, *et al.*, MitoFates: Improved prediction of mitochondrial targeting sequences and their cleavage sites. *Mol. Cell. Proteomics* **14**, 1113–1126 (2015).

68. J. J. A. Armenteros, *et al.*, Detecting sequence signals in targeting peptides using deep learning. *Life Sci. Alliance* **2**, e201900429 (2019).

69. E. F. Pettersen, *et al.*, UCSF ChimeraX: Structure visualization for researchers, educators, and developers. *Protein Sci.* **30**, 70–82 (2021).

70. I. Kawasaki, *et al.*, ASB-1, a germline-specific isoform of mitochondrial ATP synthase b subunit, is

required to maintain the rate of germline development in *Caenorhabditis elegans. Mech. Dev.* **124**, 237–251 (2007).

71. G. Tang, *et al.*, EMAN2: An extensible image processing suite for electron microscopy. *J. Struct. Biol.* **157**, 38–46 (2007).

72. A. P. Srivastava, *et al.*, High-resolution cryo-EM analysis of the yeast ATP synthase in a lipid membrane. *Science.* **360**, eaas9699 (2018).

73. T. E. Spikes, Structural studies of the mitochondrial F-ATPase (doctoral thesis). University of Cambridge. (2017) https:/doi.org/10.17863/CAM.21471 (December 7, 2022).

74. M. J. Runswick, *et al.*, The affinity purification and characterization of ATP synthase complexes from mitochondria. *Open Biol.* **3** (2012).

Data availability

The sub-tomogram averaging maps generated in this study have been deposited in the Electron Microscopy Data Bank (EMDB) under accession code EMD-16216. The source image data have been deposited to the Electron Microscopy Public Image Archive (EMPIAR) under accession number [currently unknown].

Acknowledgments

We thank Rebekah White in the lab of Cameron Weadick for sharing equipment, resources and knowledge for nematode maintenance. We acknowledge Werner Kühlbrandt at the Max-Planck Institute of Biophysics, Frankfurt, Germany, where the *S. cerevisiae* data were collected. We thank Agnieszka Chacinska at IMol Polish Academy of Sciences, Warsaw, Poland, for supporting the *S. cerevisiae* based experiments. We acknowledge access and support of the GW4 Facility for High-Resolution Electron Cryo-Microscopy, funded by the Wellcome Trust (202904/Z/16/Z and 206181/Z/17/Z) and BBSRC (BB/R000484/1), and are grateful to Ufuk Borucu of the GW4 Regional Facility for High-Resolution Electron Cryo-Microscopy for help with screening and data collection. We thank Kate Heesom from the Bristol Proteomics Facility for collecting and analysing mass spectrometry data. EB was supported by the Biotechnology and Biological Sciences Research Council-funded South West Biosciences Doctoral Training Partnership [DTP2: BB/M009122/1] awarded to VG. MM was supported by a BBSRC responsive mode grant (BB/R008639/1) grant awarded to VG. BD received funding from the European Research Council (ERC) under the European Union's Horizon 2020 research and innovation programme (grant agreement No 803894). This work was also funded by the Wellcome Trust (a Wellcome Investigator award (104632) to IC). The funders had no role in study design, data collection and interpretation, or the decision to submit the work for publication. For the purpose of Open Access, the authors have applied a CC BY public copyright license to any Author Accepted Manuscript version arising from this submission.

Author Contributions

EB conducted the experiments with *C. elegans* and analysed and quantified all tomographic data. MM assisted with electron microscopy and processing of tomographic data. PB prepared yeast mitochondria for processing by VG. AB conducted bioinformatics analysis. HF purified ATP synthase from *C. elegans* for mass spectrometry analysis. BD and PK provided resources and advice. IC and VG designed the project and obtained the funding. EB and VG wrote the paper. All authors commented on the manuscript.

Competing Interest Statement: The authors declare no competing interests.

Figures

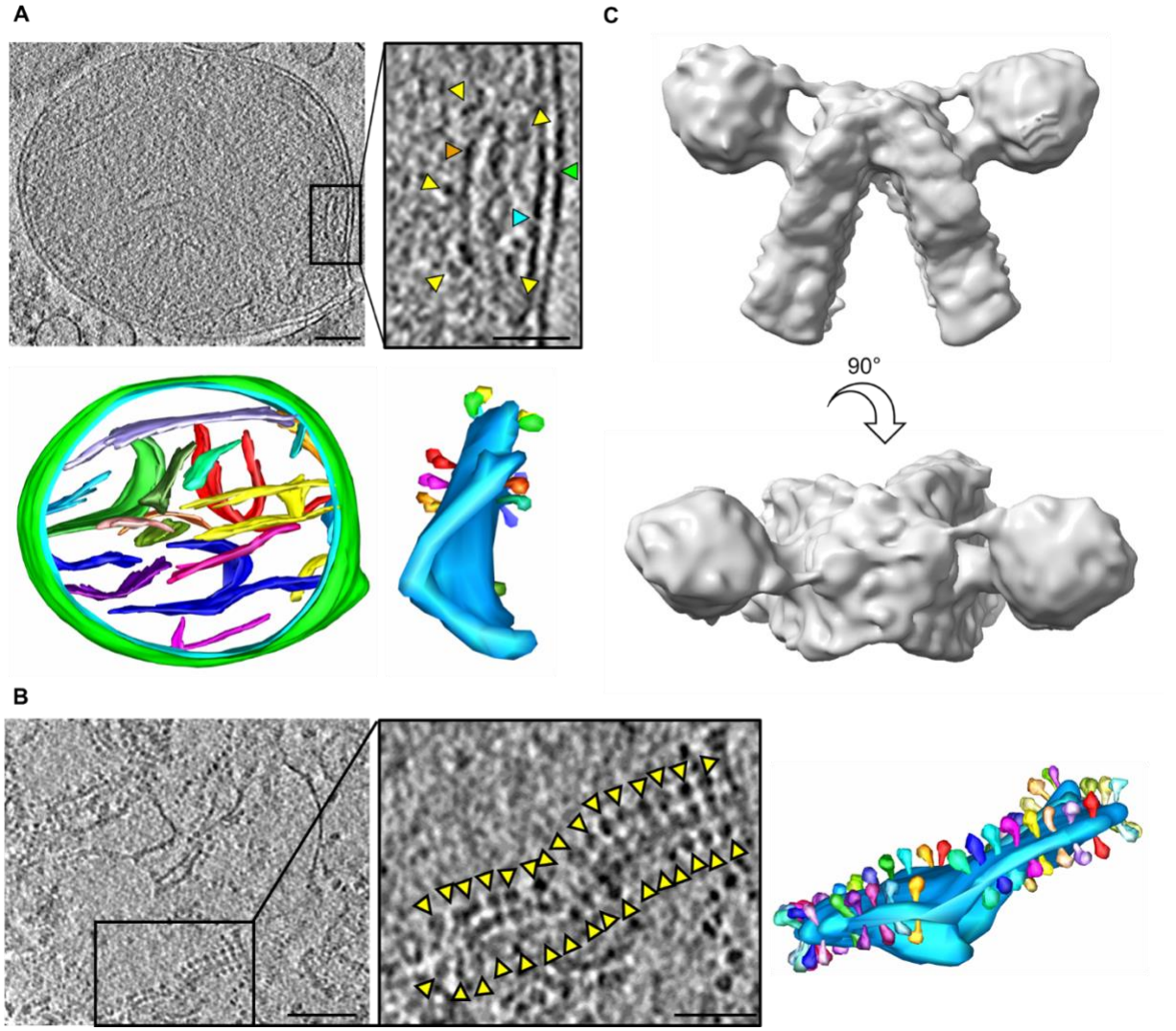

Figure 1. ATP synthase dimer rows, and sub-tomogram average of the ATP synthase dimer from *C. elegans*.

(A) Tomographic slice through a whole *C. elegans* mitochondrion (top) and corresponding segmentation (bottom; outer membrane green, inner membrane light blue, and a different colour for each crista membrane). The boxed region shows an enlarged image of a single crista membrane, with green, blue and orange arrowheads indicating the outer, inner and crista membranes respectively, and yellow arrowheads indicating ATP synthase F_1 heads. The crista membrane is coloured light blue in the corresponding segmentation; each ATP synthase dimer pair is coloured differently. **(B)** Tomographic slice through *C. elegans* isolated crista membranes (left, yellow arrowheads indicating ATP synthase F_1 heads) and

corresponding segmentation (right). The boxed region shows an enlarged image of a single crista membrane, with the corresponding segmentation coloured as in panel A. Scale bars, 100 nm for tomograms, and 50 nm for enlarged views of crista membranes. **(C)** Sub-tomogram average of the *C. elegans* ATP synthase dimer at a resolution of 38.6 Å [EMD-16216]. Upper panel shows side view, lower panel shows top down view.

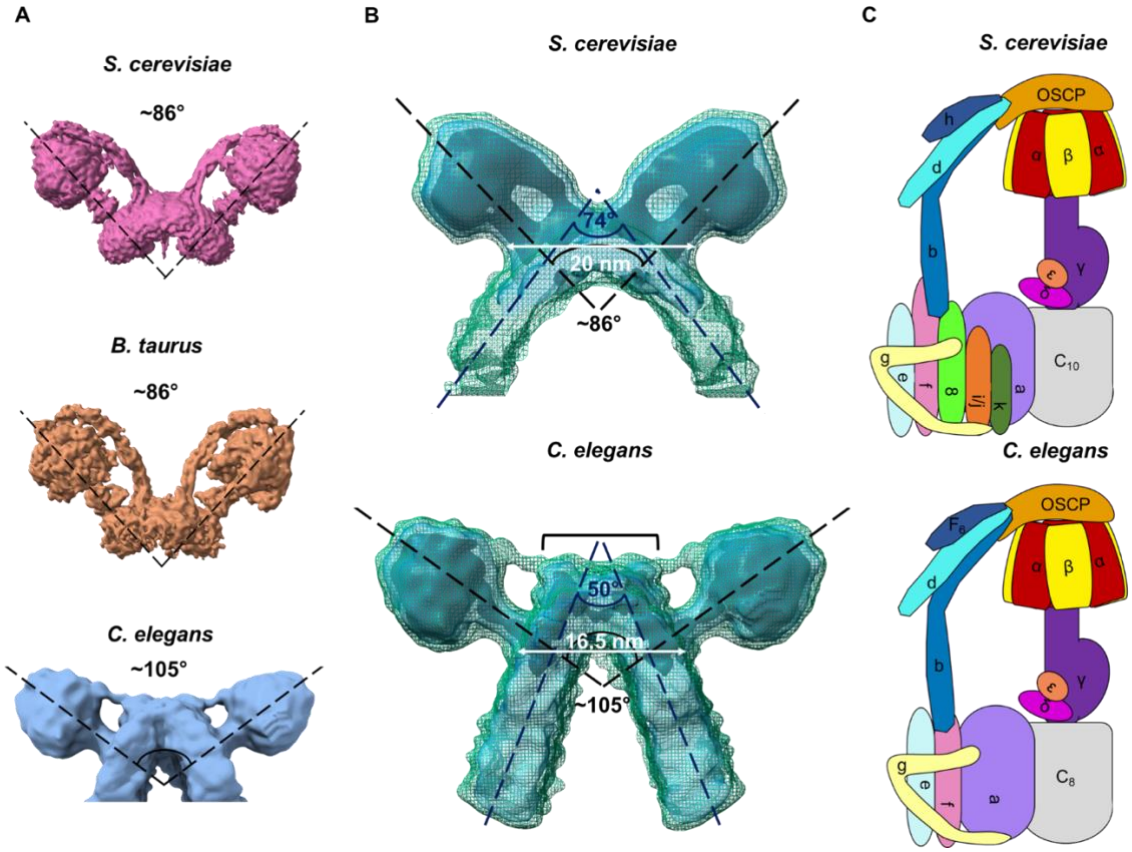

Figure 2. The *C. elegans* ATP synthase compared to other species.

(A) Structures depicting the range of average dimer angles observed in *S. cerevisiae* [EMD-7067] (30), bovine heart [EMD-11436] (29), and *C. elegans* (this work, [EMD-16216]), using the highest resolution structures available. **(B)** Direct comparison between *S. cerevisiae* [EMD-2161] (11) and *C. elegans* ATP synthase sub-tomogram averages, with the angle between F_1 dimer heads, the angle of crista membrane curvature, and crista membrane width indicated. A bracket highlights the additional density at the *C. elegans* dimer interface not apparent in *S. cerevisiae*. Black, transparent blue and dark green mesh represent decreasing threshold levels for the averages. **(C)** Cartoon detailing occurrence of ATP synthase subunits in *S. cerevisiae* and *C. elegans*, each labelled with corresponding nomenclature for the species (details in Table S1).

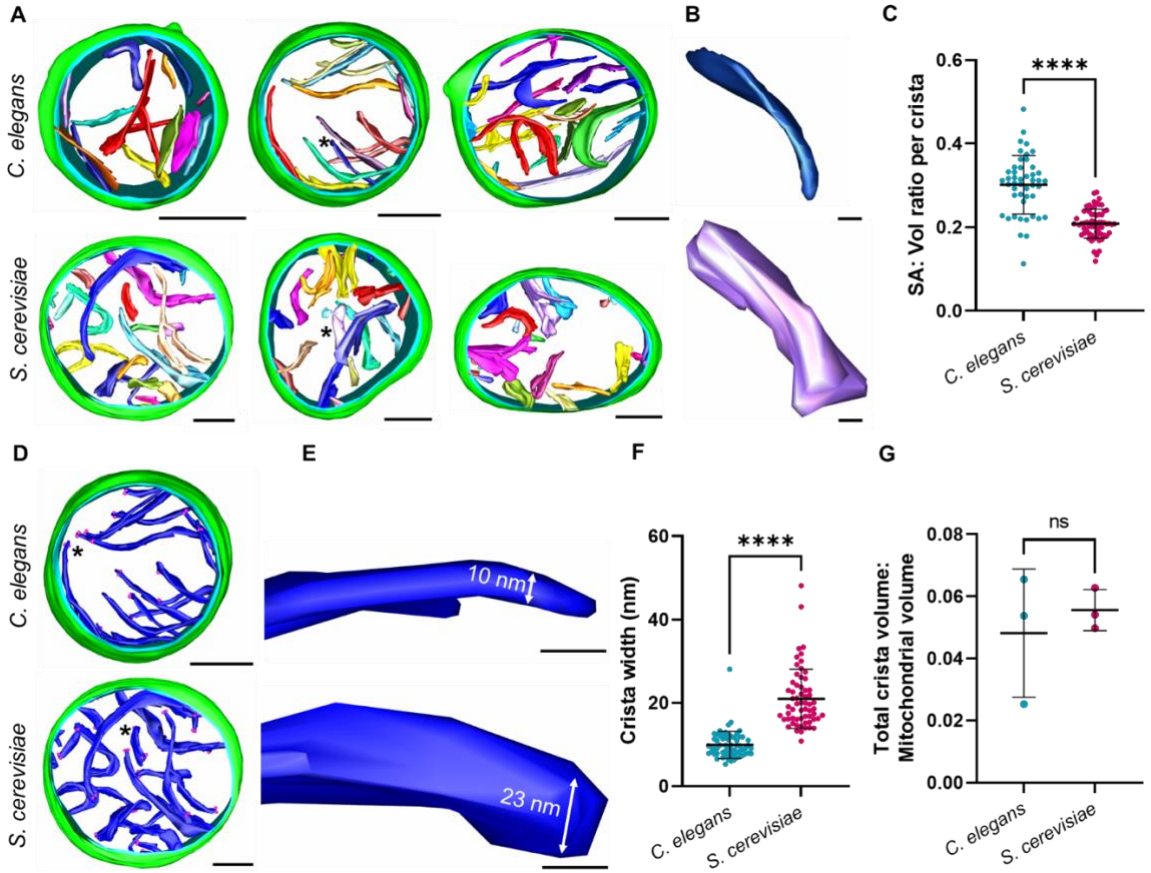

Figure 3. Morphology of mitochondria isolated from *C. elegans* and *S. cerevisiae*.

(A) Tomographic segmentations of *C. elegans* and *S. cerevisiae* mitochondria are displayed (green, outer mitochondrial membrane; blue, inner mitochondrial membrane; multi-colour, crista membranes). See Movie S1 (*C. elegans*) and Movie S2 (*S. cerevisiae*). **(B)** Enlarged examples of crista membranes (location indicated by asterisks in A) to highlight the flatter cristae morphology in *C. elegans* mitochondria compared to *S. cerevisiae*. **(C)** The mean surface area to volume ratio per crista **(**n = 3 mitochondria for each organism, with n=47 cristae for *C. elegans* and n=63 cristae for *S. cerevisiae*) was calculated from the segmentations shown in (A). **(D)** A single tomographic segmentation from each organism is shown with all crista coloured blue. Pink dots indicate distances used to measure width at the crista tips. **(E)** Close up of a single crista membrane from each organism (location indicated by asterisks in D, with crista tip width specified. **(F)** The mean crista width (n= 63 crista tips for *C. elegans* and n= 61 for *S. cerevisiae*) was calculated from the segmentations shown in (A). **(G)** The mean total crista volume relative to mitochondrial volume (n = 3 mitochondria for each organism) was calculated from the segmentations shown in (A). Error bars in C, F

and G show standard deviation of the mean and significance values were calculated using Welch's t-test for panel C or using the Mann-Whitney U-test for panels F and G. **** $p \leq 0.0001$. Scale bars in A & D, 200 nm; in B & E, 20nm.

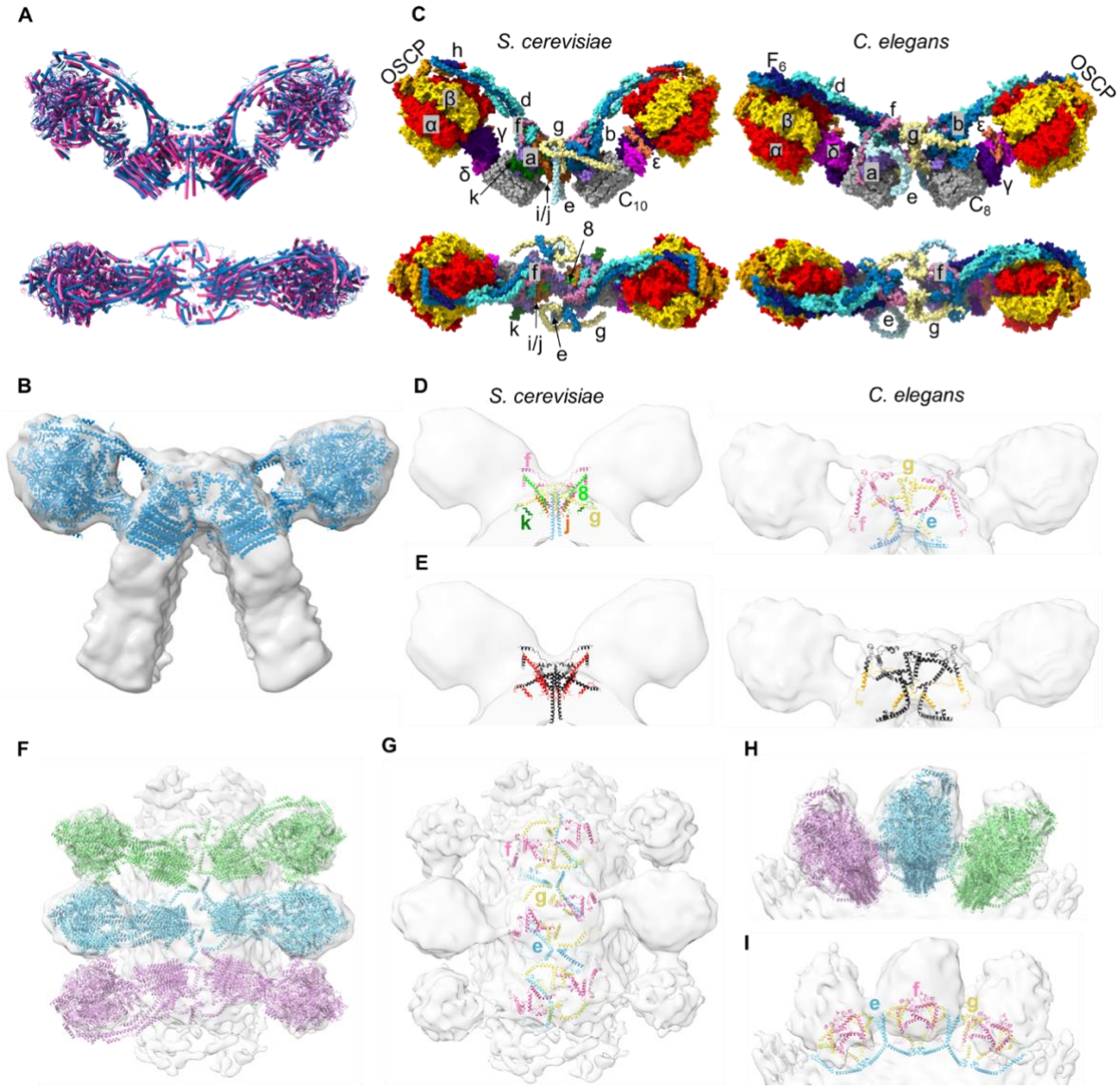

Figure 4. AlphaFold homology model of the *C. elegans* ATP synthase dimer.

(A) AlphaFold predictions for *C. elegans* ATP synthase subunits (blue) overlaid with the atomic model of the yeast ATP synthase dimer ([PDB 6B8H] (30), pink), using cylinder representation. Predicted models were fitted onto 6B8H using MatchMaker in ChimeraX. **(B)** Two monomers from the *C. elegans* ATP synthase homology model (helical representation) fitted to the sub-tomogram average of the *C. elegans* ATP synthase dimer to generate the correct dimer angle. **(C)** Surface view of *S. cerevisiae* and *C. elegans* ATP synthase dimer models coloured by chain in side (top) and top-down (bottom) views**.** Subunits are annotated and shown as α, red; β, gold; γ, indigo; δ, magenta; ε, coral; c, grey; a, purple; b, blue; d, turquoise; h/F_6, navy; OSCP, orange; e, pale blue; f, pink; g, yellow; i/j, brown; k, dark green; 8, lime. All

subunits are labelled in the side views with the exception of 8 which is buried. Only the dimer interface subunits are labelled in the top-down views. **(D)** Left, dimer interface subunits in the *S. cerevisiae* atomic model [6B8H] (30) coloured by chain and fitted to an *S. cerevisiae* sub-tomogram average [EMD-2161] (11). Right, dimer interface subunits in the *C. elegans* homology model coloured by chain fitted to the *C. elegans* sub-tomogram average. Subunits are annotated with the same colours as panel C. **(E)** As per (D), but with all subunits colored black, highlighting subunits missing in *C. elegans* relative to *S. cerevisiae* (j, k and 9) in red (left) and extensions in *C. elegans* subunits e, f and g relative to *S. cerevisiae* in orange (right). **(F)** Top down view of the *C. elegans* ATP synthase dimer homology model fitted to the sub-tomogram average showing sequential dimer pairs in a row. **(G)** As per (F), but exclusively showing dimer interface subunits e, f and g coloured by chain as per panels C and D. **(H)** and **(I)** show the same interactions as in (F) and (G) respectively but viewed from the side of a dimer row.

Supporting Information for

Cryo-electron tomography of *C. elegans* mitochondria reveals how the ATP synthase dimer interface shapes crista membranes

Emma Buzzard, Mathew McLaren, Piotr Bragoszewski, Andrea Brancaccio, Holly Ford, Bertram Daum, Patricia Kuwabara, Ian Collinson & Vicki A.M. Gold.

This PDF file includes:

- Supporting text
- Figures S1 to S12
- Tables S1 to S2
- Legends for Movies S1 to S2
- SI References

Other supporting materials for this manuscript include the following:

- Movies S1 to S2

Supporting Information Text

Extended methods

ATP synthase purification from *C. elegans* mitochondria

C. elegans ATP synthase was purified using a His-tagged IF_1 as bait, following a scaled down protocol designed for purification of bovine dimers (73, 74). Residues 1-60 of the *C. elegans* F-ATPase inhibitor protein IF_1 fused to a hexa-histindine tag (ceI1-60His), were overexpressed from a pRSFDuet plasmid in *E. coli* BL21 (DE3), and purified by affinity chromatography on a 5 mL Nickel-Sepharose column (Cytiva) attached to an ÄKTA purification system (Cytiva). Fractions enriched in IF_1 were concentrated to ~50 mg/mL with a VivaSpin concentrator (molecular weight cut-off 3 kDa; Sartorius).

C. elegans mitochondria were washed in a phosphate buffer (50 mM sodium hydrogen phosphate, 100 mM sucrose and 0.5 mM EDTA) and then centrifuged at 13,700 *x g* for 45 minutes at 4°C. This wash step was repeated twice to remove endogenous *C. elegans* IF_1. Phosphate-washed mitochondria (~16 mg) were solubilised for 30 minutes at 18°C at 7.65 mg/ml with digitonin (0.92% w/v) and DDM (0.76% w/v). The resulting extract was centrifuged at 24,000 *x g* for 20 minutes at 4°C, and ceI1-60His was added to the supernatant at 2.7 µg per 1 mg mitochondria to form ATPase:ceI1-60His complexes. A solution of 200 mM ATP, 200 mM $MgSO_4$, and 400 mM Trizma (pH 8.0) was also added at 15 µl/ml before incubating for 15 minutes at 37°C, with further additions of this solution being added at 5 minute intervals. Precipitate was removed by centrifugation at 24,000 *x g* for 10 minutes at 4°C. NaCl and imidazole were added to the clarified sample to reach final concentrations of 150 mM and 25 mM respectively. This final extract was applied to a 1 mL HisTrap FF Nickel Column (Cytiva) installed on an ÄKTA purification system (Cytiva) and equilibrated in a buffer containing 20 mM Tris, pH7.4, 150 mM NaCl, 2 mM ATP, 2 mM $MgSO_4$, 10% (v/v) glycerol, 0.1% (w/v) glyco-diosgenin (GDN) and a 0.1 mg/mL phospholipid mix. The

ATPase:ceI1-60His complexes were eluted from the column by addition of a linear gradient of imidazole up to 500 mM over 10 mL. 0.5mL fractions were collected and run on an SDS-PAGE gel to confirm which fractions contained the ATPase:I1-60His.

Nano-LC Mass Spectrometry

The sample of ATP synthase was run on a 10% SDS-PAGE gel until the dye front had migrated approximately 1cm into the separating gel. The gel lane was then excised as a single slice and subjected to in-gel tryptic digestion using a DigestPro automated digestion unit (Intavis Ltd.). The resulting peptides were fractionated using an Ultimate 3000 nano-LC system in line with an Orbitrap Fusion Lumos mass spectrometer (Thermo Scientific). Spectra were acquired with Xcalibur 3.0 software (Thermo Scientific).

The raw data files were processed and quantified using Proteome Discoverer software v2.1 (Thermo Scientific) and searched against the UniProt *Caenorhabditis elegans* database (downloaded October 2022; 26728 sequences) using the SEQUEST HT algorithm. Search criteria included oxidation of methionine (+15.995Da), acetylation of the protein N-terminus (+42.011Da) and methionine loss plus acetylation of the protein N-terminus (-89.03Da) as variable modifications and carbamidomethylation of cysteine (+57.021Da) as a fixed modification. Searches were performed with full tryptic digestion and a maximum of 2 missed cleavages were allowed. The reverse database search option was enabled and all data was filtered to satisfy false discovery rate (FDR) of 5%.

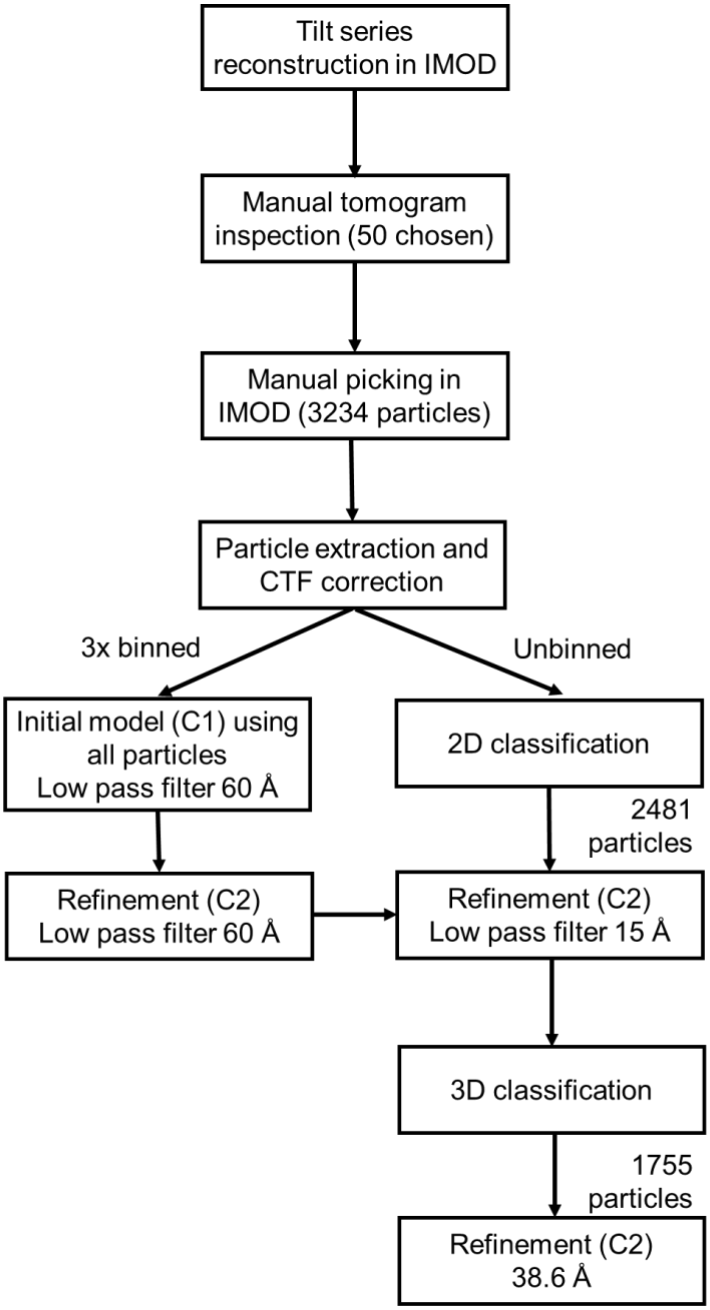

Figure S1. Flow chart of tomogram processing and sub-tomogram averaging using IMOD and Relion.

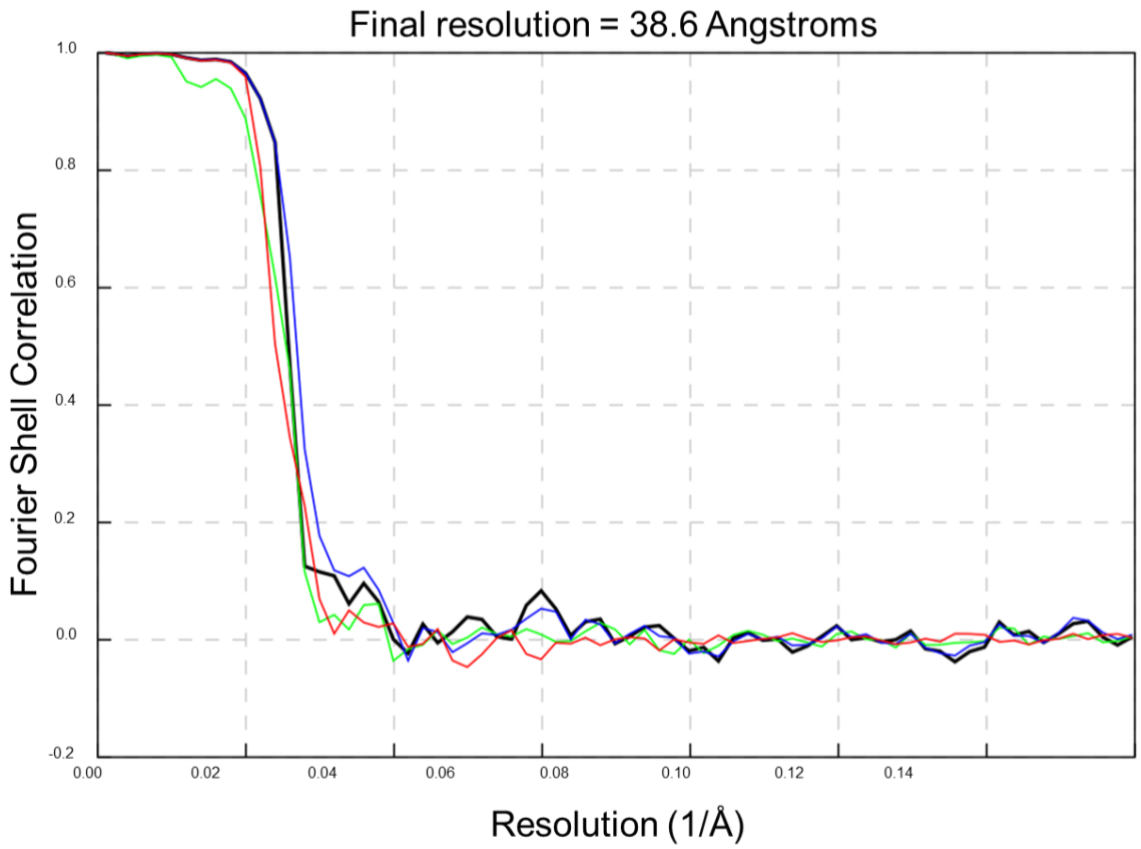

Figure S2. Fourier Shell Correlation (FSC) for the *C. elegans* ATP Synthase sub-tomogram averaging map. The FSC curve is an output from Relion 3.1. The corrected FSC is shown in black, unmasked FSC in green, masked FSC in blue, and phase randomised masked FSC in red.

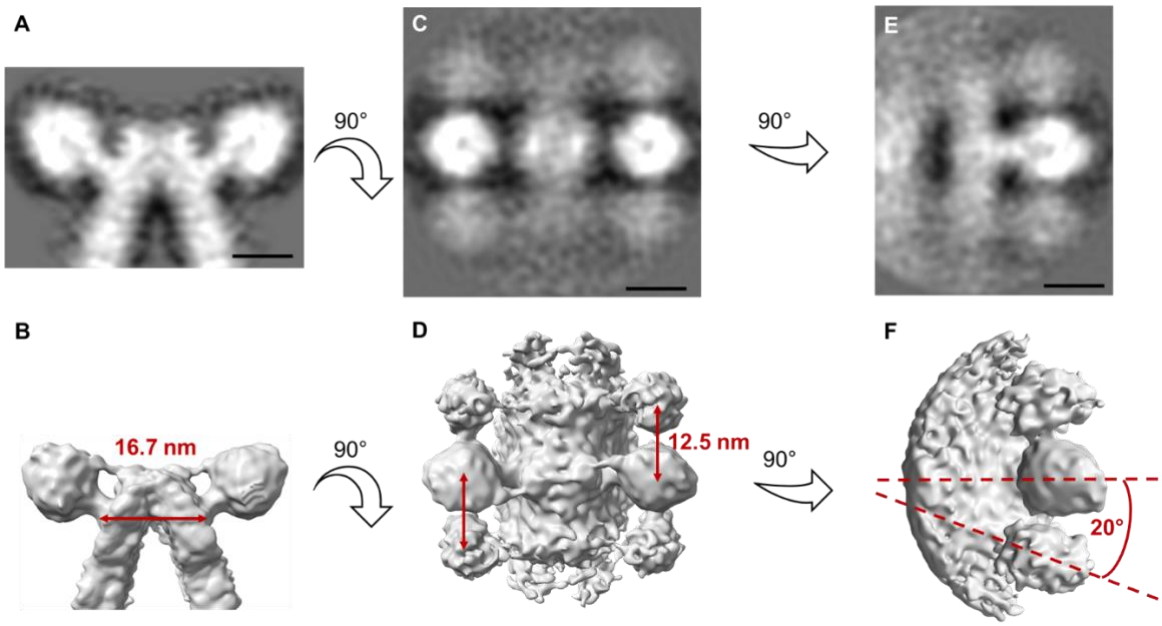

Figure S3. Inter-dimer distance and angle between consecutive dimer heads in oligomeric rows of *C. elegans* ATP synthase dimers. (A) 2D projection showing side view of a masked map of the *C. elegans* ATP Synthase dimer. **(B)** Side view shown in 3D, with distance between central stalks indicated. **(C)** 2D projection showing top down view of an unmasked map of the *C. elegans* ATP synthase dimer. **(D)** Top down view in 3D with inter-dimer distance indicated. **(E)** 2D projection showing side view (rotated 90° compared to A) of an unmasked map of the *C. elegans* ATP Synthase dimer. **(F)** Side view in 3D, with inter-dimer angle indicated. All indicated measurements were made in IMOD. Scale bars, 10 nm.

Subunit e

```
tr|Q21732|Q21732_CAEEL      MSAPLKHPNAVVLQPPTVTISPLIRFGRYAALSLGVVYGFFRLRQIREYHADIREWDH-E      59
sp|P81449|ATPJ_YEAST        --------------------MSTVNVLRYSALGLGLFFGFRNDMILKCNAKKKEEQAQYE      40
sp|Q00361|ATP5I_BOVIN       -------------MVPPVQVSPLIKLGRYSALFLGMAYGAKRYNYLKPRAEEERRLAA-E      46
                                                :.. **:** **: :*  .   ::    . ..    *

tr|Q21732|Q21732_CAEEL      KAVAAAEEAAKKKKWLAKD-----------EMRYLMQVVNIPFEEGVKQFGVADLYKED-      107
sp|P81449|ATPJ_YEAST        EKLKLVEEAK---KEYAKLHPVVTPKDVPANASFNLEDPNIDFERVIL--NAVESLKEAS      95
sp|Q00361|ATP5I_BOVIN       EKKKRDEQK-RIERELAEA-----------QEDTILK----------------------      71
                            :     *:     :  *:           :    ::

tr|Q21732|Q21732_CAEEL      -   107
sp|P81449|ATPJ_YEAST        T   96
sp|Q00361|ATP5I_BOVIN       -   71
```

Subunit f

```
sp|Q22021|ATPK_CAEEL        MAWFRPPPPHTQLRPWVPDAIFIPISRAVERVGVFFYNRVLNKTEVGLFDKRWNKNVHGP  60
sp|Q06405|ATPK_YEAST        MI-------------------F---KRAV---STLIPPKVVSS-----------------  18
sp|Q28851|ATPK_BOVIN        ------------------------------------------------------------  0

sp|Q22021|ATPK_CAEEL        YCHWRYYGKLDTKFMDVKLGDLPAWM------ARREKTPSAFYNE--FMRNIWRVHNLYY  112
sp|Q06405|ATPK_YEAST        ----------------KNIGSAPNAKRIANVVHFYKSLPQGPAPAIKANTRLARYKAKYF  62
sp|Q28851|ATPK_BOVIN        --MASVVPLKEKKLLEVKLGELPSWI------LMRDFTPSGIAGA--FQRGYYRYYNKYV  50
                                                ::*. *            .  *..            *    *

sp|Q22021|ATPK_CAEEL        SGPVYNNTVKVIFRF-----IFAYSFLNWLVKSHRYVDFQKTMYHW        153
sp|Q06405|ATPK_YEAST        DGDNA--SGKPLWHFALGIIAFGYSMEYYFHLR----HHKGAEEH-        101
sp|Q28851|ATPK_BOVIN        NVK--KGSIAGLSMV-----LAAYVFLNYCRSYKELKHERLRKYH-        88
                            .      :   :  .       .* :  :        . :    *
```

Subunit g (isoform 2)

```
sp|Q18803|ATPL2_CAEEL       MAAPKLGFFEKIANLTGALYRHQHAQFPRR-------F-AILKAVGKHELAPPRQADWPA 52
sp|Q12233|ATPN_YEAST        -------MLSRIQNYTSGLVSKANLLSSKALYYGKVGAEISKQIYLKEGLQPPTVAQFKS 53
sp|Q28852|ATP5L_BOVIN       ----MAEFVRNLAEKAPALVNAAVTYSKPR-------L-ATFWYYAKVELVPPTPAEIPT 48
                                  :. .: : : .*                          *  * **  *:  :

sp|Q18803|ATPL2_CAEEL       IKADWAKV-QSF-----IQTGGYKNLSIREGLVYTAVTLEVVFWFFVGEMIGRRYIFGYL 106
sp|Q12233|ATPN_YEAST        VYSNLYKQSLNFALKPTEVLSCLKNIQKNELLKYGAYGIQLIGFYSVGEIIGRRKLVGYK 113
sp|Q28852|ATP5L_BOVIN       AIQSLKKI-INS-----AKTGSFKQLTVKEALLNGLVATEVWMWFYVGEIIGKRGIIGYD 102
                               .  *   .         .  *::  .* *       ::  :: ***:**:* :.**

sp|Q18803|ATPL2_CAEEL       VPADYVSKSTKKTVKEQEALAALEN    131
sp|Q12233|ATPN_YEAST        HH-----------------------   115
sp|Q28852|ATP5L_BOVIN       V-----------------------    103
```

Subunit b (isoform 2)

```
sp|Q19126|AT5F2_CAEEL      MSLSRCLPLGQNARVIIIPARLAHAASTQAAAATDDAPNFFQKLAHRFQGVPLKGEAHAP 60
sp|P05626|ATPF_YEAST       MSM-----------------SM------------------------GVRGLALR---SVS 16
sp|P13619|AT5F1_BOVIN      MLS-----------------RV------------------------VLS--AAA---AAA 14
                           *                   :                         .          .

sp|Q19126|AT5F2_CAEEL      KSMFEDCNKEWSAPEPLPAIPKDFKEHPDRDLVNYPYPARPMYPPKSRLLMMPDSWFTPF 120
sp|P05626|ATPF_YEAST       KTLFSQG---VRCPSMVIGA----RYM-SSTPEKQT---DPKAKANSIINAIPGN---NI 62
sp|P13619|AT5F1_BOVIN      PSLKNAA---LLGPGVLQAT----RIFHTGQPSLAPVPPLPEHGGKVRFGLIPEEFFQFL 67
                            :: .        *  : .     :               *    :  :  :* .    :

sp|Q19126|AT5F2_CAEEL      QKVTGVSGPYLFFGGLFAFLVNKELWVFEEQGHMTVGWILFYLLVTRTAGYKIDQGLYNG 180
sp|P05626|ATPF_YEAST       LTKTGVLG---TSAAAVIYAISNELYVINDESILLLTFLGFTGLVAKYLAPAYK-----D 114
sp|P13619|AT5F1_BOVIN      YPKTGVTGPYVLGTGLILYLLSKEIYVITPETFSAISTIGFLVYIVKKYGASVG-----E 122
                              *** *      . . : :.:*::*:  :    :  : *   :.:  .

sp|Q19126|AT5F2_CAEEL      YQERVNF--------FKGLIQEDLKEAVEFKKTSAKQTESLNSIKESYPTALKESMALQL 232
sp|P05626|ATPF_YEAST       FADARMKKVSDVLNASRNKHVEAVKDRID----SVSQLQNVAETTKVLFDVSKETVELES 170
sp|P13619|AT5F1_BOVIN      FADKLNEQKIAQLEEVKQASIKQIQDAID----MEKSQQALVQKRHYLFDVQRNNIAMAL 178
                           : :             :    : ::: ::      .. : : .  .    . ::.: :

sp|Q19126|AT5F2_CAEEL      EATYRKNVQSVATELKRRIDYLKETEESKARVEREQLLKLINSEVDKEFSDRSFKDKYLQ 292
sp|P05626|ATPF_YEAST       EAFELKQKVELAHEAKAVLDSWVRYEASLRQLEQRQLAKSVISRVQSELGNPKFQEKVLQ 230
sp|P13619|AT5F1_BOVIN      EVTYRERLHRVYREVKNRLDYHISVQNMMRQKEQEHMINWVEKRVVQSISAQQE-KETIA 237
                           *.   :.   :  * *  :*     :    : *:.:: : : ..* ..:.  .  .: :

sp|Q19126|AT5F2_CAEEL      NAIQQLKGLNVQL------  305
sp|P05626|ATPF_YEAST       QSISEIEQLLSKLK-----  244
sp|P13619|AT5F1_BOVIN      KCIADLKLLSKKAQAQPVM  256
                           :.* ::: *  :
```

Subunit d

```
tr|Q17763|Q17763_CAEEL     MSGAAKRVATSSVNWSKLAER--LVPEHAAELTRVKGVSGTFQSAVSQLPADLPKIDFAA      58
sp|P30902|ATP7_YEAST       --MSLAKSAANKLDWAKVISSLRITGSTATQLSSFKKRNDEARRQLLELQSQPTEVDFSH      58
sp|P13620|ATP5H_BOVIN      --MAGRKLALKTIDWVAFGEI--IPRNQKAVANSLKSWNETLTSRLATLPEKPPAIDWAY      56
                              :  : * ..::*  . .   :  .  :  . .*  .      :  *  .   :*::

tr|Q17763|Q17763_CAEEL     LKKALPAHSA--VLDSLQKQYESVKIPYGEVPAEYL---------KEVDQWVDYNNARIK      107
sp|P30902|ATP7_YEAST       YRSVLKNTSVIDKIESYVKQYKPVKIDASKQLQ-------------VIESFEKHAMTNAK      105
sp|P13620|ATP5H_BOVIN      YKANV-AKAG--LVDDFEKKFNALKVPIPEDKYTAQVDAEEKEDVKSCAEFLTQSKTRI-      112
                            :  :   :    ::.  *::: :*:   :                   .:     :.

tr|Q17763|Q17763_CAEEL     LHEVKVADGLQEAKKVEEKWAKAPPVEHFDRQHFVEYFPAHFYDLRYQNRIPDPCNIGLN      167
sp|P30902|ATP7_YEAST       ETESLVSKELKDLQSTLDNIQSARPFDELTVDDLTKIKPEIDAKVEE------MVKKGKW      159
sp|P13620|ATP5H_BOVIN      ----------QEYEKELEKMRNIIPFDQMTIEDLNEVFPETKLDKKKYPYWPHRPIETL-      161
                                     :: :.  ::  .  *.:.:  :.: :  *    . .

tr|Q17763|Q17763_CAEEL     ETPEIENRFKDYKVLRRADKVDDH    191
sp|P30902|ATP7_YEAST       DVPGYKDRFGNLNVM---------    174
sp|P13620|ATP5H_BOVIN      ------------------------    161
```

Subunit F_6

```
tr|O16517|O16517_CAEEL      -----MFRAVQSV----RS---L-------ST---TAACRQDLIQQTFVTKIREIAK---      35
sp|Q12349|ATP14_YEAST       -----MFPIASRRILLNASVLPLRLCNRNFTTTRISY----NVIQDLYLRELKDTKLAPS      51
sp|P02721|ATP5J_BOVIN       MILQRLFRLSSAV----QSAISV-SWRRNIGITAVAFNKELDPVQKLFVDKIREYRTK--      53
                                 :*   .       *   :            :     : :*. :: ::::

tr|O16517|O16517_CAEEL      ----NAGNLANSDPAVKKALQEELNRLATKFQLANADVVSKLPTNFEAAKVDSAVQSALE      91
sp|Q12349|ATP14_YEAST       TLQDAEGNVKPWNPPQKPNLPELELQ-----GPEALKAYTE--QNVETAHVA---KESEE      101
sp|P02721|ATP5J_BOVIN       --RQTSGGPVDAGPEYQQDLDRELFKLKQMYGKADMNTFPN--FTFEDPKFEVVE-----      104
                                 *.    .*  :  * .   :          ..  :   ..*  :.

tr|O16517|O16517_CAEEL      GQTLASLLEGVKKD-HSEYVASRDAKKAEQAARNAALKQ     129
sp|Q12349|ATP14_YEAST       ---------GESEPIEEDWLVLDDAEETKESH-------     124
sp|P02721|ATP5J_BOVIN       ------------KP-QS---------------------     108
                                        :  ..
```

Subunit OSCP

```
tr|P91283|P91283_CAEEL      MAQ-------LMKRGFSTS--AALAKAQLVKTPIQVHGVEGRYAAALYSAGHKQNKLDQI      51
sp|P05626|ATPF_YEAST        ------MSMSMGVRGLALRSVSKTLFSQGVRCPSMVIGA--RYMSST---PEKQT-----      44
sp|P13621|ATPO_BOVIN        MAALAVSGLSQQVRCFSTS--VVRPFAKLVRPPVQIYGIEGRYATALYSAASKQNKLEQV      58
                                      * ::         :: *: *  : *   ** ::      **.

tr|P91283|P91283_CAEEL      STDLNNVRSVYKDNKKFQEFVLDPTLKANKK----------KTAIEAI------------      89
sp|P05626|ATPF_YEAST        ------------DPKAKANSIINAIPGNNILTKTGVLGTSAAAVIYAISNELYVINDESI      92
sp|P13621|ATPO_BOVIN        EKELLRVGQILKEPKM-AASLLNPYVKRSVK----------VKSLSDM------------      95
                                    : *     :::     .               :  :

tr|P91283|P91283_CAEEL      --STKLGLTKETGNFLGLLA---ENGRLNKLESVV------------SSFESI---MRAH      129
sp|P05626|ATPF_YEAST        LLLTFLGFTGLVAKYLAPAYKDFADARMKKVSDVLNASRNKHVEAVKDRIDSVSQLQNVA      152
sp|P13621|ATPO_BOVIN        --TAKEKFSPLTSNLINLLA---ENGRLTNTPAVI------------SAFSTM---MSVH      135
                               :   ::  ..: :        :.*:.:   *:            . :.::     .

tr|P91283|P91283_CAEEL      -RGELFVQVTS-AEELSSS-----NQK----ALSDALSKIGKSGQKLT-V-TYAVKPSIL      176
sp|P05626|ATPF_YEAST        ETTKVLFDVSKETVELESEAFELKQKVELAHEAKAVLDSWVRYEASLRQLEQRQLAKSVI      212
sp|P13621|ATPO_BOVIN        -RGEVPCTVTT-ASALDEA-----TLT----ELKTVLKSFLSKGQVLK-L-EVKIDPSIM      182
                               ::   *:. :  *..               . .*..       *  :    :  *::

tr|P91283|P91283_CAEEL      GGLVVTIGD-----KYVDLSIASRVKKYKDALATAI        207
sp|P05626|ATPF_YEAST        SRVQSELGNPKFQEKVLQQSIS-EIEQLLSKLK---        244
sp|P13621|ATPO_BOVIN        GGMIVRIGE-----KYVDMSAKTKIQKLSRAMREIL        213
                            . :   :*:     * :: *   .:::    :
```

Figure S4. Multiple sequence alignment for dimer interface and peripheral stalk subunits. Comparisons were made between *C. elegans* (O16517), *S. cerevisiae* (Baker's yeast strain ATCC 204508 / S288c; Q12349) and *B. taurus* (P02721) using Clustal Omega at EMBL-EBI (47–49). In the alignment output, an asterisk (*) indicates a perfect alignment, a colon (:) indicates a site belonging to a group exhibiting strong similarity, and full stop (.) indicates a site belonging to a group exhibiting weak similarity. Residues are coloured according to their biophysical properties.

Small and hydrophobic residues are coloured red, acidic residues are coloured blue, basic residues are coloured magenta, and hydroxyl, sulfhydryl, amine and glycine residues are coloured green. Extensions in *C. elegans* subunits relative to both the *S. cerevisiae* and *B. taurus* homologues are underlined in black, deletions are underlined in maroon. Where subunits have multiple isomers, the isomer used in the homology model is used for alignment.

Subunit e (Q21732)

MSAPLKHPNAVVLQPPTVTISPLIRFGRYAALSLGVVYGFFRLRQIREYHADIREWDHEKAVAAAE
EAAKKKKWLAKDEMRYLMQVVNIPFEEGVKQFGVADLYKED

Subunit f (Q22021)

MAWFRPPPPHTQLRPWVPDAIFIPISRAVERVGVFFYNRVLNKTEVGLFDKRWNKNVHGPYCH
WRYYGKLDTKFMDVKLGDLPAWMARREKTPSAFYNEFMRNIWRVHNLYYSGPVYNNTVKVIFR
FIFAYSFLNWLVKSHRYVDFQKTMYHW

Subunit g (isoform 2) (Q18803)

MAAPKLGFFEKIANLTGALYRHQHAQFPRRFAILKAVGKHELAPPRQADWPAIKADWAKVQSFIQ
TGGYKNLSIREGLVYTAVTLEVVFWFFVGEMIGRRYIFGYLVPADYVSKSTKKTVKEQEALAALE
N

Subunit b (isoform 2) (Q19126)

MSLSRCLPLGQNARVIIIPARLAHAASTQAAAATDDAPNFFQKLAHRFQGVPLKGEAHAPKSMFE
DCNKEWSAPEPLPAIPKDFKEHPDRDLVNYPYPARPMYPPKSRLLMMPDSWFTPFQKVTGVSG
PYLFFGGLFAFLVNKELWVFEEQGHMTVGWILFYLLVTRTAGYKIDQGLYNGYQERVNFFKGLIQ
EDLKEAVEFKKTSAKQTESLNSIKESYPTALKESMALQLEATYRKNVQSVATELKRRIDYLKETEE
SKARVEREQLLKLINSEVDKEFSDRSFKDKYLQNAIQQLKGLNVQL

Subunit d (Q17763)

MSGAAKRVATSSVNWSKLAERLVPEHAAELTRVKGVSGTFQSAVSQLPADLPKIDFAALKKALP
AHSAVLDSLQKQYESVKIPYGEVPAEYLKEVDQWVDYNNARIKLHEVKVADGLQEAKKVEEKWA

KAPPVEHFDRQHFVEYFPAHFYDLRYQNRIPDPCNIGLNETPEIENRFKDYKVLRRADKVDDH

Subunit F_6 (O16517)

MFRAVQSVRSLSTTAACRQDLIQQTFVTKIREIAKNAGNLANSDPAVKKALQEELNRLATKFQLA
NADVVSKLPTNFEAAKVDSAVQSALEGQTLASLLEGVKKDHSEYVASRDAKKAEQAARNAALKQ

Figure S5. Mass spectrometry data for *C. elegans* ATP synthase subunits with significant extensions. The sequence for each subunit of interest is shown and identified with a Uniprot code. The predicted mitochondrial targeting sequences are coloured red. The *C. elegans* specific extensions (revealed in sequence alignments from Fig. S4) are highlighted in yellow. Peptides identified by mass spectrometry are underlined. Where subunits have multiple isomers, the isomer used in the homology model is shown.

Alphafold predictions gallery

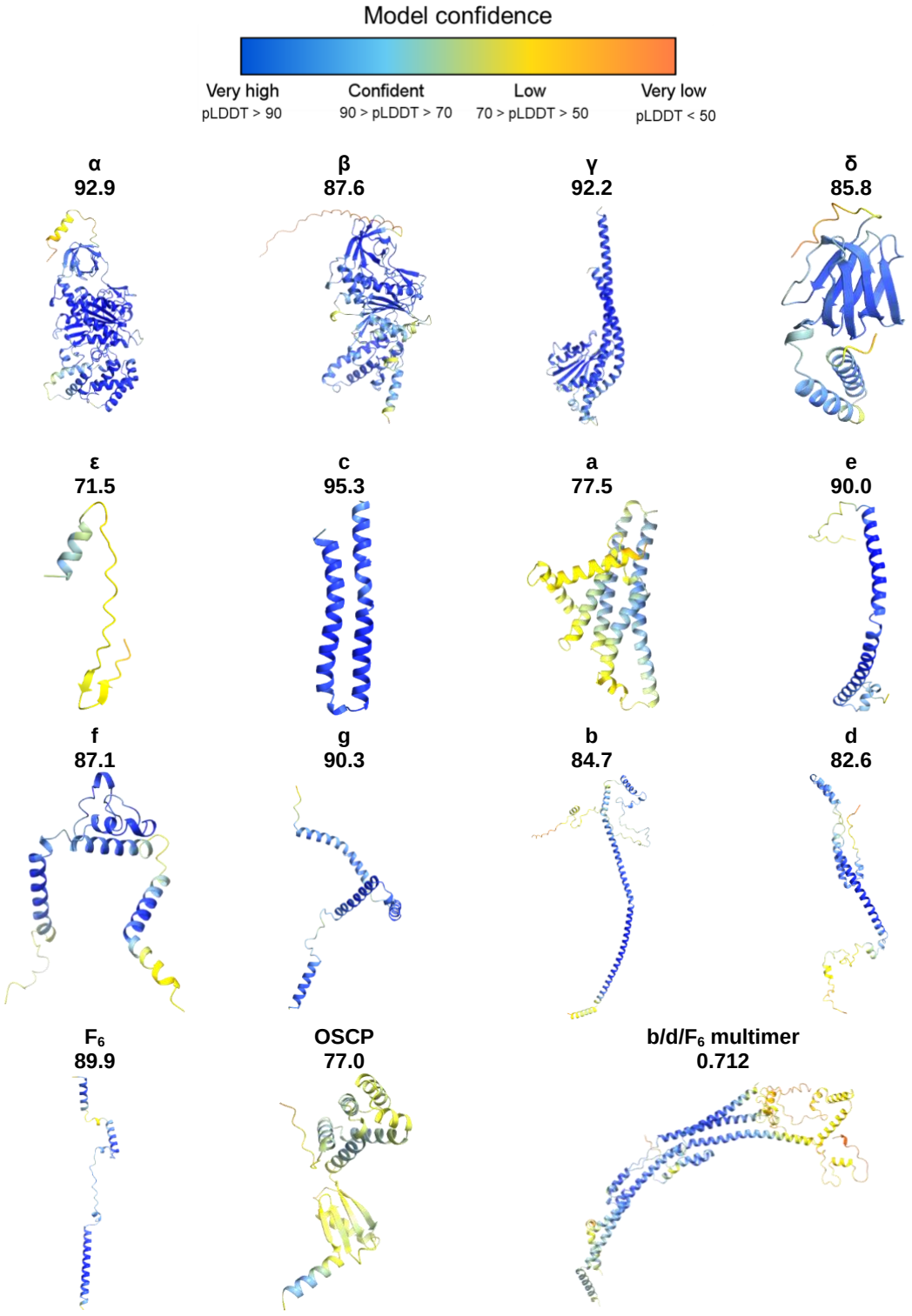

758

Figure S6. AlphaFold predictions gallery

AlphaFold predictions (41) for each *C. elegans* ATP synthase subunit, coloured by pLDDT score per residue. The pLDDT score is a per-residue measure of local confidence on a scale from 0 – 100. The structure of subunits b d and F_6 were predicted as a multimer. The confidence measure for predictions made using AlphaFold multimer (50) is similar, but modified to score interactions between residues of different chains. It is calculated using a weighted combination of predicted-TM score (pTM) and interface predicted-TM score (ipTM), and has a scale from 0-1. The appropriate mean confidence score for each AlphaFold / multimer prediction is shown beneath each subunit name.

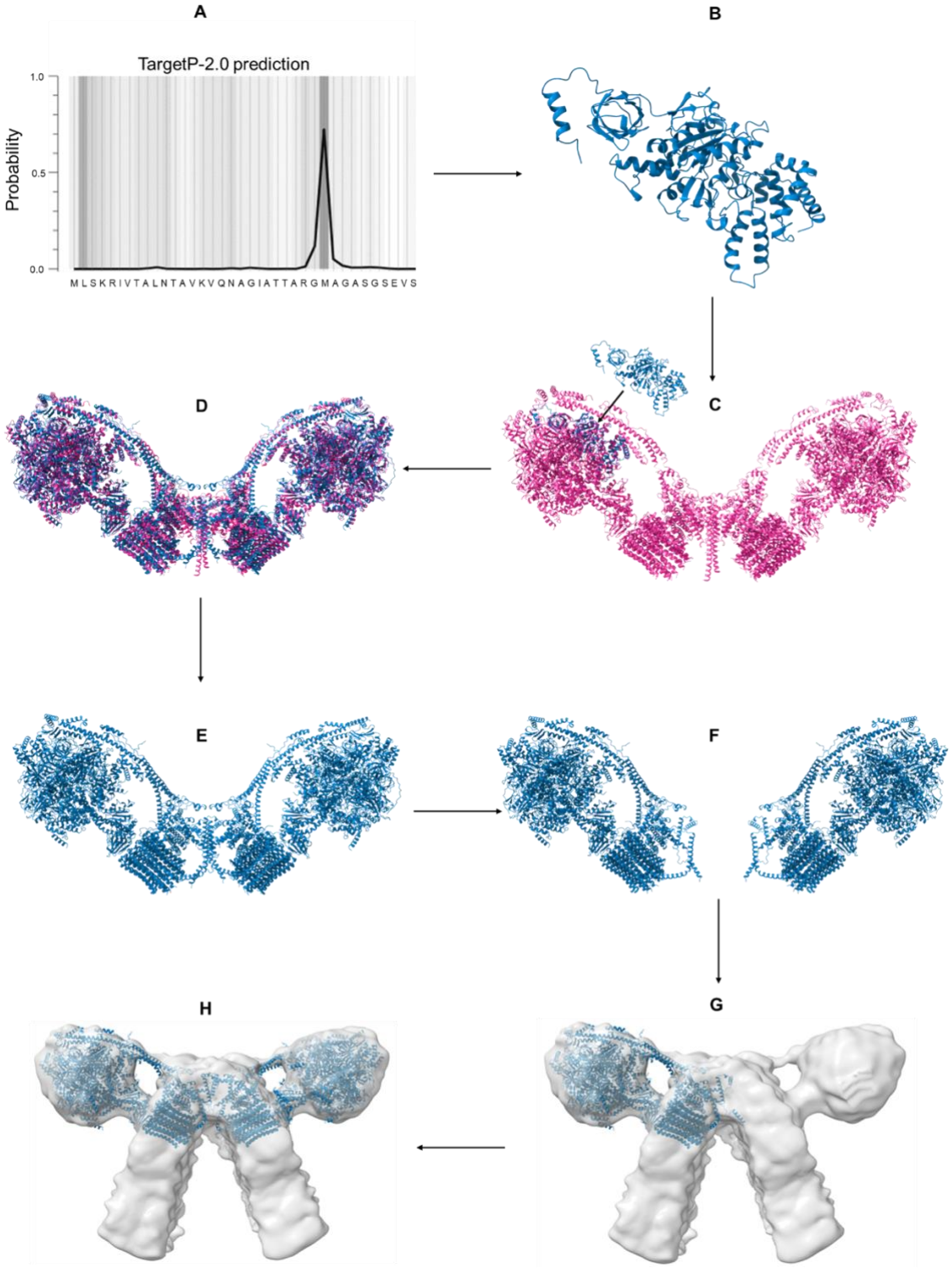

Figure S7. *C. elegans* ATP synthase homology model workflow

(A) MitoFates (67) or TargetP-2.0 (68) were used to predict the mitochondrial targeting sequence

of individual proteins of the ATP synthase, so that the mature protein sequence could be identified. The example shown is the TargetP-2.0 prediction for subunit α. **(B)** AlphaFold was used to predict structures of all mature *C. elegans* ATP synthase subunits; again the example shown is the prediction for subunit α. **(C)** Predicted models were sequentially fitted into the *S. cerevisiae* ATP synthase model [PDB 6B8H] (30) using MatchMaker in ChimeraX. **(D)** The resulting homology model (blue) after all subunits have been fitted to the scaffold provided by 6B8H (pink). **(E)** The homology model without the *S. cerevisiae* scaffolding. **(F)** The *C. elegans* ATP synthase dimer was split into separate monomers. **(G)** The monomers were fitted sequentially into the sub-tomogram average of the *C. elegans* ATP synthase using matchmaker in ChimeraX in order to obtain the correct dimer angle. **(H)** The final homology model of the *C. elegans* ATP synthase dimer fitted into the sub-tomogram average.

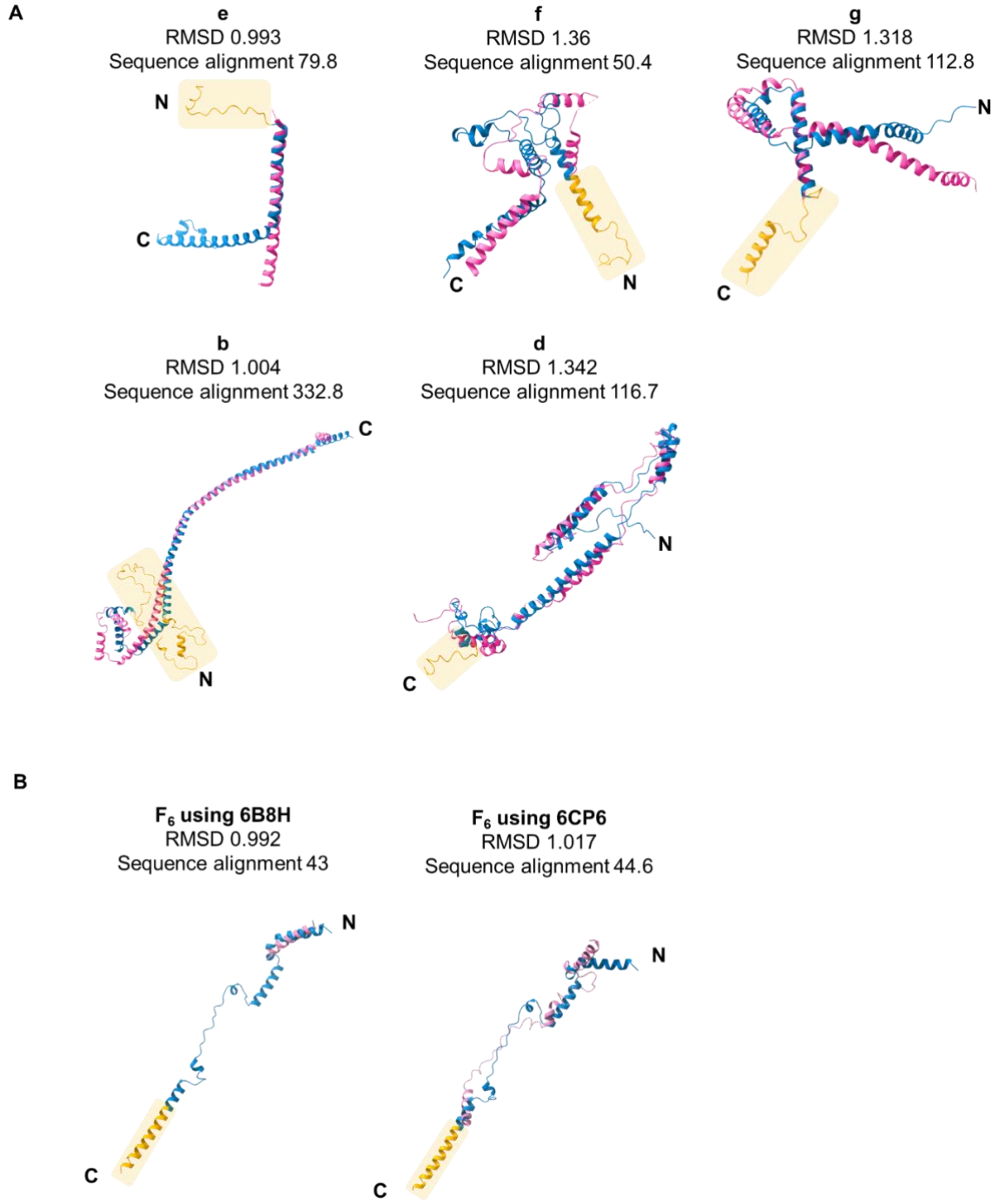

Figure S8. Overlays of individual subunits at the dimer interface and peripheral stalk, where there are extensions in *C. elegans* homologues compared with *S. cerevisiae*. *C. elegans* AlphaFold predictions (blue) are overlaid with their *S. cerevisiae* counterparts (6B8H, pink) (30). *C. elegans* subunit extensions are highlighted in orange. RMSD values (for pruned atom pairs) and

sequence alignment scores output by ChimeraX when using the “fit to model” tool are shown for each overlay. **(A)** Overlays for subunits e, f, g, b and d are taken from the assembled ATP synthase dimers in Fig. 4A. **(B)** Two alternative overlays are shown for subunit F_6. Left, an overlay taken from Fig. 4A as above. However, the *S. cerevisiae* 6B8H (30) structure does not contain the complete density for subunit F_6. Right, an *S. cerevisiae* monomeric atomic model [PDB 6CP6] (72) was used to display a more complete *S. cerevisiae* chain for the overlay.

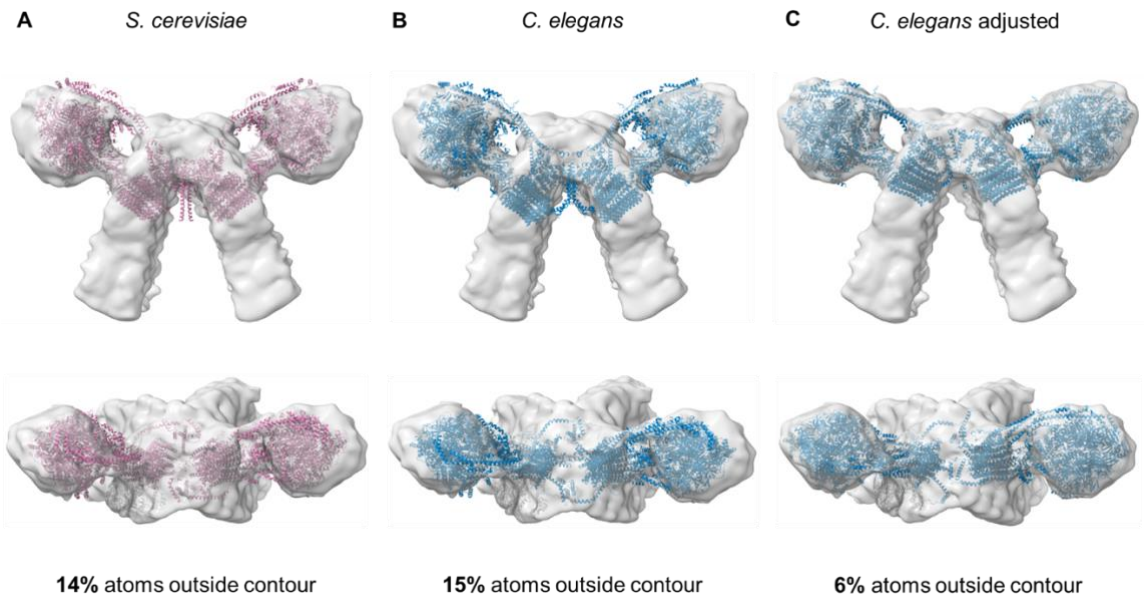

Figure S9. Comparison of different models fitted to the *C. elegans* ATP synthase dimer map. Different ATP synthase dimer models were fitted into the *C. elegans* ATP synthase *in situ* map. All models were fitted into the map at threshold 0.0429 in ChimeraX, and the percentage of atoms outside the contour is shown for each model. **(A)** The purified *S. cerevisiae* ATP synthase dimer atomic model [PDB 6B8H] (30) shows a poor fit, with 14% of atoms outside the contour. **(B)** The *C. elegans* ATP synthase dimer homology model following scaffolding to the *S. cerevisiae* model also shows a poor fit, with 15% of atoms outside the contour. **(C)** Sequential fitting of monomers from the *C. elegans* homology model shows an improved fit, with only 6% of atoms outside the contour.

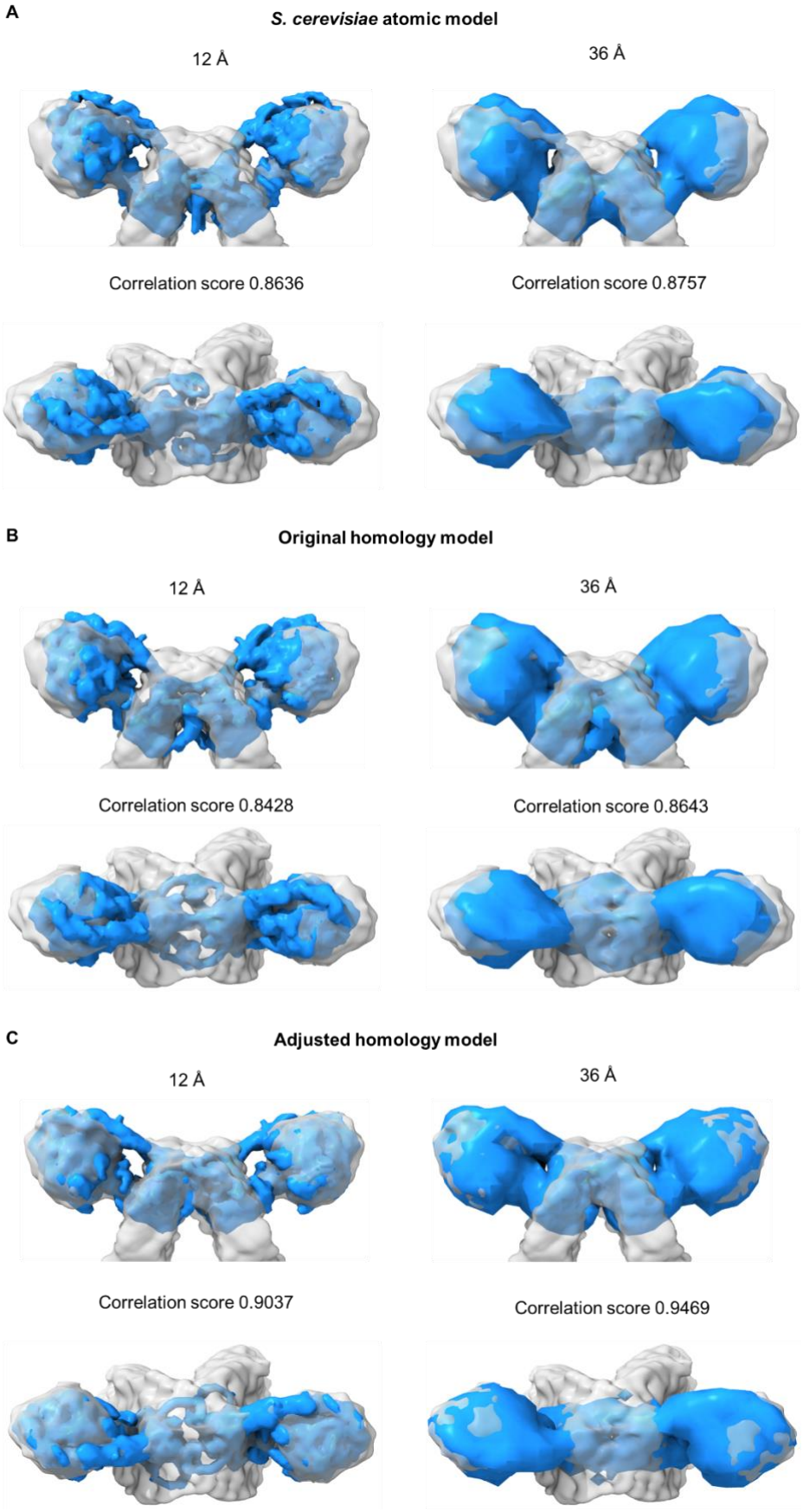
A
S. cerevisiae atomic model
12 Å
36 Å
Correlation score 0.8636
Correlation score 0.8757
B
Original homology model
12 Å
36 Å
Correlation score 0.8428
Correlation score 0.8643
C
Adjusted homology model
12 Å
36 Å
Correlation score 0.9037
Correlation score 0.9469

806

Figure S10. The *C. elegans* homology model fitted to the *C. elegans* ATP synthase dimer sub-tomogram averaging map. Using the pdb2mrc command in EMAN2 (71), the PDB of the *C. elegans* homology model was converted into an MRC map at both 12 Å and 36 Å resolution. Converted pdb2mrc maps (blue) were then fitted to the sub-tomogram averaging map of the *C. elegans* dimer (grey) at equivalent threshold levels. Correlation scores between the homology model and sub-tomogram averaging maps are displayed. **(A)** Maps of the 6B8H *S. cerevisiae* ATP synthase atomic model (30) fitted to the sub-tomogram average for reference**. (B)** Maps of the *C. elegans* original homology model (without adjusting for dimer angle) fitted to the sub-tomogram average. **(C)** Maps of the dimer angle adjusted *C. elegans* homology model fitted to the sub-tomogram average**.**

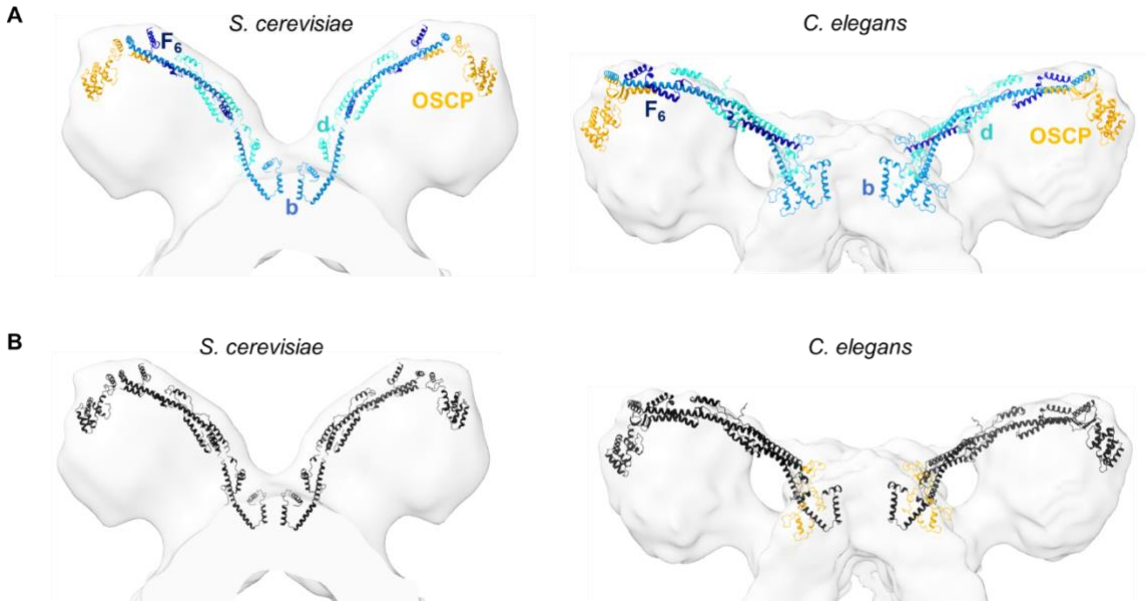

Figure S11. Comparison of peripheral stalk subunit arrangement in *S. cerevisiae* vs *C. elegans* ATP synthase dimers. (A) *S. cerevisiae* and *C. elegans* peripheral stalk subunits coloured by chain. Subunits are annotated and shown as b, blue; d, turquoise; F_6, dark navy; and OSCP, orange. Left, peripheral stalk subunits b, d and OSCP in the 6B8H *S. cerevisiae* atomic model (30), and F_6 from the 6CP6 monomeric atomic model (72), fitted to the *S. cerevisiae* sub-tomogram average [EMD-2161] (11). The chain for F_6 was taken from EMD-6CP6 (see Fig. S8B) (72). Right, *C. elegans* homology model fitted to the *C. elegans* sub-tomogram average. **(B)** As per (A), but with all subunits colored black, highlighting extensions in *C. elegans* subunits b, d and F_6 relative to *S. cerevisiae* in orange.

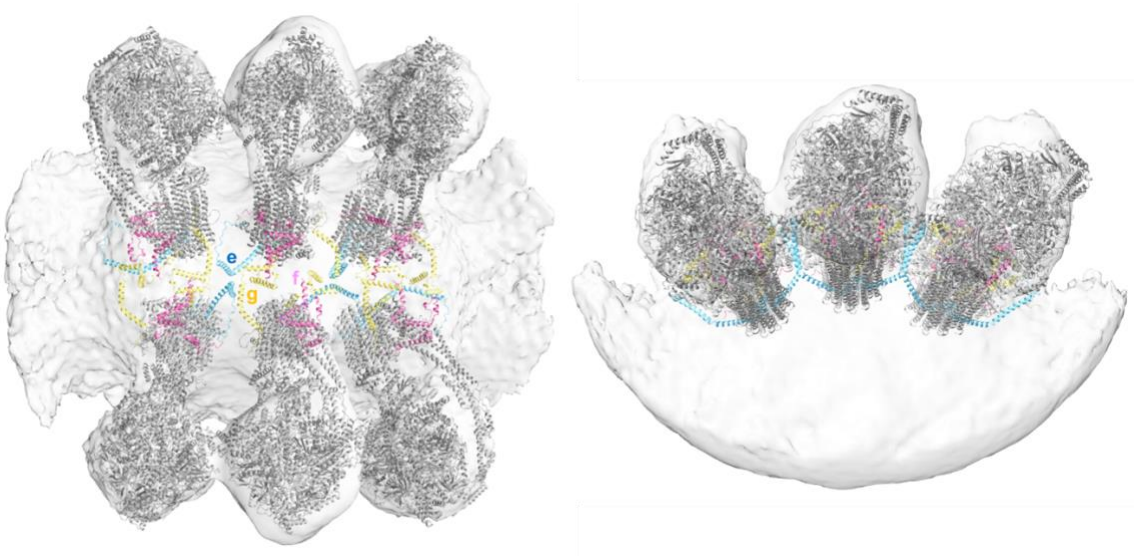

Figure S12. Inter-dimer interactions mediated by subunits e and g in *C. elegans* ATP synthase dimer rows. Top down view (left) and side view (right) of the *C. elegans* ATP synthase homology model (grey) fitted to each dimer pair in the unmasked sub-tomogram average of the *C. elegans* dimer. Dimer interface subunits are colored (e, pale blue; f, pink; g, yellow) to highlight extensive inter-dimer interactions mediated by subunits e and g.

Table S1. Nomenclature for homologues of ATP Synthase subunits

C. elegans	*S. cerevisiae*	*B. taurus*
F_1 head		
α	α/Atp1	α
β	β/Atp2	β
F_o head		
γ	γ/Atp3	γ
δ	δ/Atp16	δ
ε	ε/Atp15	ε
Peripheral stalk		
b	b/Atp4	b
d	d/Atp7	d
F_6	h/Atp14	F_6
OSCP	OSCP/Atp5	OSCP
F_o motor		
a	a/Atp6	a
c	c/Atp9	c
Type I dimer-specific subunits		
e	e/Atp21	e
f	f/Atp17	f
g	g/Atp20	g
-	i/j/Atp18	6.8PL/ j
-	k/Atp19	DAPIT/ k
-	8/Atp8	A6L/ATP8

Nomenclature for yeast and mammalian species are described as detailed by Song and Pfanner (6).

Table S2. Metrics to assess confidence and fit of AlphaFold predicted structures

Subunit name	*C. elegans* Uniprot Accession Number	Mean pLDDT (or weighted pTM & ipTM)[1]	RMSD between pruned atom pairs[2]	RMSD across all atom pairs	Sequence alignment score[3]
α	Q9XXK1	92.9066444	0.929	2.275	1869.6
β	P46561	87.5983733	1.241	2.961	1875.8
γ	Q95XJ0	92.17635904	0.914	2.058	665.4
δ	Q09544	85.82596715	0.901	2.488	224.7
ε[4]	O16298	65.4116052			
	P34539	71.51756013	0.541	15.704	18.9
c	Q9BKS0	95.27668763	0.74	0.74	262.1
e	Q21732	89.96603434	0.993	10.078	79.8
f	Q22021	87.12810426	1.36	14.559	50.4
g	Q18803	90.2590889	1.318	10.538	112.8
a	P24888	77.54888203	1.154	4.824	308.5
b	Q20053	84.43326886			
	Q19126	84.74422485	1.004	15.512	332.8
d	Q17763	82.60642993	1.342	9.967	116.7
F_6	O16517	89.9038886	0.992	15.452	43
OSCP	P91283	76.95722866	1.035	7.553	346.3
	Q7JNG1	76.43462181			
b,d,F_6 multimer	Q19126, Q17763, O16517	0.712090029	1.324	11.335	327.9

[1] pLDDT scores are shown for subunits where structure was predicted individually, a weighted pTM and iPTM score is shown for a complex of subunits predicted using AlphaFold multimer. The pLDDT score is a per-residue measure of local confidence on a scale from 0 – 100. The predicted-TM score (pTM) and interface predicted-TM score (ipTM), and has a scale from 0-1.

[2] RMSD (Root Mean Square Deviation) is a measure of the similarity between two superimposed atomic coordinates, in this case for the predicted *C. elegans* subunits and the model of the *S. cerevisiae* ATP synthase dimer.

[3] Sequence alignment score between *C. elegans* and *S. cerevisiae.*

[4] Where a subunit has more than one isoform, the version with the highest pLDDT score was used to build the homology model. RMSD and sequence alignment scores are only shown for the selected protein. In the case of subunit b, the isoform with the highest pLDDT score is also the only isoform expressed in somatic tissues (70).

Movie S1 (separate file). Movie showing a 360° rotation about the y-axis of a single segmented *C. elegans* mitochondrion from the upper panel of Fig. 3A. An image sequence of 100 PNG files was collected in IMOD, and the sequence montaged into a10fps AVI file in Image J (64).

Movie S2 (separate file). Movie showing a 360° rotation about the y-axis of a single segmented *S. cerevisiae* mitochondrion from the lower panel of Fig. 3A. An image sequence of 100 PNG files was collected in IMOD, and the sequence montaged into a10fps AVI file in Image J (64).

SI References

6. J. Song, N. Pfanner, T. Becker, Assembling the mitochondrial ATP synthase. *Proc. Natl. Acad. Sci. USA.* **115**, 2850–2852 (2018).

11. K. M. Davies, C. Anselmi, I. Wittig, J. D. Faraldo-Gómez, W. Kühlbrandt, Structure of the yeast F 1 F o -ATP synthase dimer and its role in shaping the mitochondrial cristae. *Proc. Natl. Acad. Sci. USA.* **109**, 13602–13607 (2012).

30. H. Guo, S. A. Bueler, J. L. Rubinstein, Atomic model for the dimeric F_o region of mitochondrial ATP synthase. *Science.* **358**, 936–940 (2017).

41. J. Jumper, *et al.*, Highly accurate protein structure prediction with AlphaFold. *Nature* **596**, 583–589 (2021).

47. F. Sievers, *et al.*, Fast, scalable generation of high-quality protein multiple sequence alignments using Clustal Omega. *Mol. Syst. Biol.* **7**, 539 (2011).

48. M. Goujon, *et al.*, A new bioinformatics analysis tools framework at EMBL-EBI. *Nucleic Acids Res.* **38**, W695–W699 (2010).

49. H. McWilliam, *et al.*, Analysis Tool Web Services from the EMBL-EBI. *Nucleic Acids Res.* **41**, W597-W600 (2013).

50. R. Evans, *et al.*, Protein complex prediction with AlphaFold-Multimer. *bioRxiv* (2021) https:/doi.org/10.1101/2021.10.04.463034 (November 30, 2021).

64. C. A. Schneider, W. S. Rasband, K. W. Eliceiri, NIH Image to ImageJ: 25 years of image analysis. *Nat. Methods* **9**, 671–675 (2012).

67. Y. Fukasawa, *et al.*, MitoFates: Improved Prediction of Mitochondrial Targeting Sequences and Their Cleavage Sites. *Mol. Cell. Proteomics* **14**, 1113–1126 (2015).

68. J. J. A. Armenteros, *et al.*, Detecting sequence signals in targeting peptides using deep learning. *Life Sci. Alliance* **2**, e201900429 (2019).

70. I. Kawasaki, *et al.*, ASB-1, a germline-specific isoform of mitochondrial ATP synthase b subunit, is required to maintain the rate of germline development in *Caenorhabditis elegans. Mech. Dev.* **124**, 237–251 (2007).

71. G. Tang, *et al.*, EMAN2: An extensible image processing suite for electron microscopy. *J. Struct. Biol.* **157**, 38–46 (2007)

72. A. P. Srivastava, *et al.*, High-resolution cryo-EM analysis of the yeast ATP synthase in a lipid membrane. *Science* **360** (2018).

73. T. E. Spikes, Structural studies of the mitochondrial F-ATPase (doctoral thesis). University of Cambridge. (2017) https:/doi.org/10.17863/CAM.21471 (December 7, 2022).

74. M. J. Runswick, *et al.*, The affinity purification and characterization of ATP synthase complexes from mitochondria. *Open Biol.* **3** (2012).